JEM Journal of Experimental Medicine

ARTICLE

IL-17A–producing γδT cells promote muscle regeneration in a microbiota-dependent manner

Alexander O. Mann[1,2*], Bola S. Hanna[1,2*], Andrés R. Muñoz-Rojas[1,2], Inga Sandrock[3], Immo Prinz[3,4], Christophe Benoist[1,2], and Diane Mathis[1,2]

Subsequent to acute injury, skeletal muscle undergoes a stereotypic regenerative process that reestablishes homeostasis. Various types of innate and adaptive immunocytes exert positive or negative influences at specific stages along the course of muscle regeneration. We describe an unanticipated role for γδT cells in promoting healthy tissue recovery after injection of cardiotoxin into murine hindlimb muscle. Within a few days of injury, IL-17A–producing γδT cells displaying primarily Vγ6$^+$ antigen receptors accumulated at the wound site. Punctual ablation experiments showed that these cells boosted early inflammatory events, notably recruitment of neutrophils; fostered the proliferation of muscle stem and progenitor cells; and thereby promoted tissue regeneration. Supplementation of mice harboring low numbers of IL-17A$^+$ γδT cells with recombinant IL-17A largely reversed their inflammatory and reparative defects. Unexpectedly, the accumulation and influences of γδT cells in this experimental context were microbiota dependent, unveiling an orthogonal perspective on the treatment of skeletal muscle pathologies such as catastrophic wounds, wasting, muscular dystrophies, and myositides.

Introduction

Skeletal muscle injury provokes a tightly coordinated, highly effective regenerative process (Charge and Rudnicki, 2004). For example, intramuscular injection of myotoxins such as cardiotoxin (CTX) induces acute muscle-fiber necrosis, which results in the rapid recruitment and/or activation of diverse innate and adaptive immunocyte populations, culminating in inflammation. Concomitantly, muscle stem cells (MuSCs), quiescent before injury, are mobilized to proliferate and differentiate (Sambasivan et al., 2011; Lepper et al., 2011). The resulting muscle precursor cells (MPCs) fuse with each other and with existing myofibers to regenerate healthy muscle tissue. This highly stereotypic process normally takes about 2 wk.

MuSC proliferation and differentiation are strongly influenced by the local inflammatory response to tissue damage, distinct phases of the regenerative process being supported by either its pro- or anti-inflammatory stages (Tidball, 2017). The initial proliferation of MuSCs is promoted by inflammatory cytokines such as TNFα and IFNγ; however, these same cytokines are detrimental to subsequent differentiation events (Arnold et al., 2007; Cheng et al., 2008; Chen et al., 2007; Villalta et al., 2011; Londhe and Davie, 2011; Londhe and Davie, 2013). Anti-inflammatory macrophages (MFs) and regulatory T cells (Tregs) support the reparative phase of myogenesis following the initial inflammatory/proliferative phase (Segawa et al., 2008; Tonkin et al., 2015; Varga et al., 2016; Deng et al., 2012; Burzyn et al., 2013; Villalta et al., 2014; Castiglioni et al., 2015; Kuswanto et al., 2016; Panduro et al., 2018).

While exploring the role of Tregs in skeletal muscle regeneration, we noticed an impressive accumulation of γδT cells 3 d after CTX injury, which had not previously been reported. Here, we address the role of γδT cells in the regenerative process subsequent to acute muscle injury. We found that a prominent population of IL-17A$^+$ γδT cells promoted early inflammation and subsequent tissue regeneration in an IL-17A– and microbiota-dependent manner. These findings suggest new targets for the experimental and therapeutic modulation of muscle repair.

Results

IL-17A–producing γδT cells accumulate in skeletal muscle following acute injury

Flow cytometric analysis revealed a small population of local γδT cells at steady state, which expanded greatly in response to acute injury of hindlimb muscle via CTX injection (Fig. 1, A and

[1]Department of Immunology, Harvard Medical School, Boston, MA; [2]Evergrande Center for Immunologic Diseases, Harvard Medical School and Brigham and Women's Hospital, Boston, MA; [3]Institute of Immunology, Hannover Medical School, Hannover, Germany; [4]Institute of Systems Immunology, University Medical Center Hamburg-Eppendorf, Hamburg, Germany.

*A.O. Mann and B.S. Hanna contributed equally to this paper. Correspondence to Diane Mathis: dm@hms.harvard.edu.

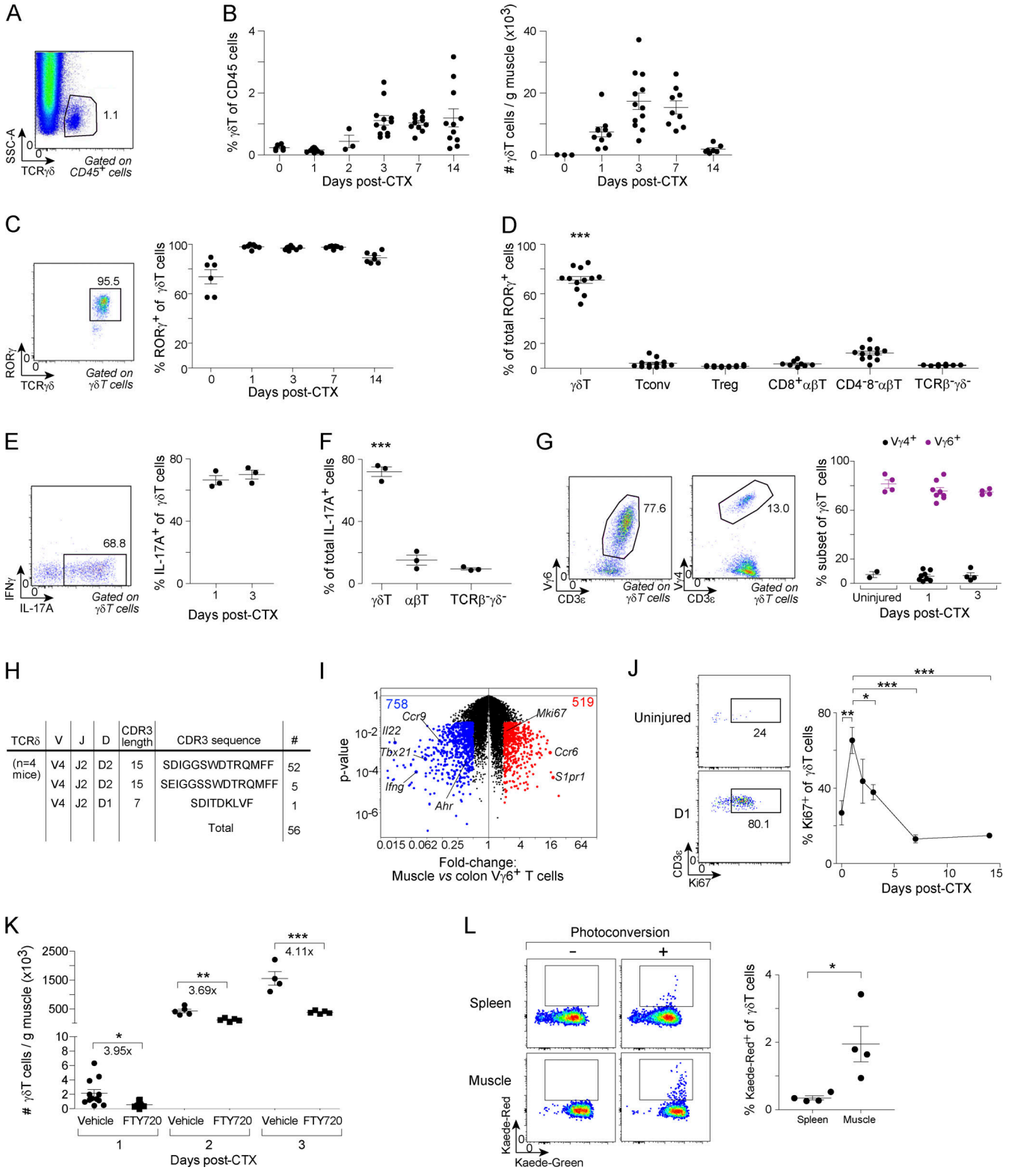

Figure 1. **Acute muscle injury induces the accumulation of IL-17A⁺ γδT cells. (A and B)** Flow cytometric data on TCRγδ expression by immunocytes from hindlimb muscle of mice after CTX-induced injury. **(A)** Representative dot-plot of day 3 data. SSC, side scatter. **(B)** Summary data over time for fractional representation (left) and numbers (right) of γδT cells. **(C)** Flow cytometric analysis of RORγ expression by γδT cells from injured muscle. Left: Representative dot-plot of day 3 data. Right: Summary data for RORγ⁺ γδT cell frequency over time. **(D)** Flow cytometric data on RORγ expression by diverse cells of the muscle T-lymphocyte compartment on day 3 after injury. Data in A–D were compiled from two to three independent experiments. **(E)** Flow cytometric analysis of IL-17A expression by muscle γδT cells following PMA + ionomycin stimulation. Left: Representative dot-plot of day 3 data. Right: Summary data over time of IL-17A production. **(F)** Flow cytometric data on IL-17A expression by diverse cells of the muscle T-lymphocyte compartment on day 3 after injury. Representative of two independent experiments. **(G)** Flow cytometric analysis of Vγ6⁺ and Vγ4⁺ muscle T cells. Left: Representative plots of Vγ6⁺ (left) and Vγ4⁺

(right) staining; Right: Summary plot. **(H)** Sequencing data on the *Trdv4* complementarity-determining region 3 (CDR-3) of individually sorted Vγ6⁺ T cells from muscle 3 d after injury. **(I)** Volcano plot illustrating transcriptional differences between Vγ6⁺ γδT cells from the colonic lamina propria and 3-d injured muscle (n = 3). Values at the top indicate the number of transcripts significantly (P < 0.05) up-regulated (red) and down-regulated (blue) ≥2-fold in injured muscle. **(J)** Flow cytometric analysis of Ki67 expression by muscle γδT cells. Left: Representative dot-plots of uninjured and day 1 data. Right: Summary data for Ki67⁺ cell frequency among γδT cells. Data obtained from two to three independent experiments. **(K)** Flow cytometric quantification of γδT cells in skeletal muscle at different days after injury; mean FC values between experimental conditions at each time point are annotated above. Data obtained from three independent experiments. **(L)** Flow cytometric quantification of Kaede-Red and Kaede-Green fluorescence signal from spleen and muscle γδT cells 3 d after cervical lymph node photoconversion and hindlimb skeletal muscle injury. Tconv, CD4⁺ Foxp3⁻ conventional T cell; Treg, CD4⁺ Foxp3⁺ regulatory T cell. All plots: means ± SEM; *, P < 0.05; **, P < 0.01; ***, P < 0.001 by unpaired t test.

B). The numerical peak occurred on day 3, but the fractional representation remained elevated for ≥14 d. γδT cells are often broadly divided into IFNγ- and IL-17A–producing subsets (Chien et al., 2014). Virtually all of the γδT cells in injured muscle expressed the transcription factor, RORγ (Fig. 1 C), and γδT cells constituted the majority of all RORγ⁺ lymphocytes in muscle on day 3 after injury (Fig. 1 D). RORγ is a major driver of IL-17A production (Cua and Tato, 2010); accordingly, there was robust staining of IL-17A in muscle γδT cells following injury, with almost undetectable staining of IFNγ (Fig. 1 E). γδT cells comprised the majority of all IL-17A⁺ cells in the muscle 3 d after injury (Fig. 1 F).

γδT cells differentiate in the thymus in developmentally timed waves, which are characterized by distinct T cell receptor (TCR) rearrangements and phenotypes (Chien et al., 2014). In mice, IL-17–producing γδT cells display Vγ6⁺ or Vγ4⁺ TCRs (Wei et al., 2015). Vγ6⁺ cells emerge around the time of birth and have essentially invariant TCRs, whereas Vγ4⁺ cells differentiate postnatally and possess more diverse TCRs. Following injury, Vγ6⁺ cells accounted for the vast majority of γδT cells accumulating in skeletal muscle, although a minor population of Vγ4⁺ cells was also detectable (Fig. 1 G). The fractions of Vγ6⁺ versus Vγ4⁺ γδT cells did not significantly change after injury, at least during the time frame examined (Fig. 1 G). To determine whether the dominating Vγ6⁺ cells underwent canonical TCR rearrangements, we sorted individual Vγ6⁺ cells and sequenced their Vδ1 (*Trdv4*) transcripts to assess the extent of junctional diversity, which is where any diversity usually occurs in Vγ6⁺ TCRs (Lafaille et al., 1989; Holtmeier et al., 2010; Fig. 1 H). More than 90% of the sequenced Vγ6⁺Vδ1⁺ cells carried the canonical Vδ1 rearrangement, consistent with what we and others have observed for Vγ6⁺Vδ1⁺ cells from WT mice (O'Brien and Born, 2015; Fujikado et al., 2016).

To more broadly assess the phenotype of muscle Vγ6⁺ T cells, specifically in comparison with a better-characterized population of IL-17A–producing γδT cells, we sorted Vγ6⁺ cells from the muscle 3 d after injury and from the colonic lamina propria (Wei et al., 2015; Lee et al., 2015) and performed RNA sequencing (RNA-seq; Fig. 1 I). Hundreds of transcripts were up- or down-regulated in the muscle vis-a-vis colonic cells, although no particular gene sets emerged as differential upon application of standard pathway analysis programs. Compared with those in the colon, Vγ6⁺ cells from injured muscle expressed fewer transcripts encoding the cytokines IL-22 and IFNγ, as well as fewer transcripts specifying the transcription factors that promote expression of these cytokines, Ahr and Tbx21, respectively (Martin et al., 2009; Barros-Martins et al., 2016). At the transcript level, *Il17a* was expressed highly by both muscle and colonic Vγ6⁺ cells (Fig. S1 A). Notably, but not unexpectedly, there were also differences between these two populations of Vγ6⁺ cells in the expression of mRNAs encoding receptors associated with cell-trafficking. Muscle cells expressed more *Ccr6* and *S1pr1*, but less *Ccr9*, encoding the gut-homing receptor (Wurbel et al., 2001; Fig. 1 I). The muscle and colon Vγ6⁺ populations expressed similar levels of transcripts encoding the cytokine receptors IL-1R and IL-23R, as well as some chemokine receptors previously reported to regulate Tγδ17 trafficking, notably CCR2 and CXCR6 (Fig. S1 B; Duan et al., 2010; Sutton et al., 2009; Martin et al., 2009; McKenzie et al., 2017; Akitsu et al., 2015; Alves de Lima et al., 2020). By multiple criteria, then, the γδT cells present in skeletal muscle following acute injury appeared to be a prototypical Tγδ17 population. They were the dominant source of IL-17 in injured muscle.

We then explored the extent to which the accumulation of muscle γδT cells reflected local expansion of a tissue-resident population versus recruitment from a circulating pool. Muscle injury did induce cell cycle entry, as measured by Ki-67 expression, an effect that was most pronounced on day 1 after injury and gradually decreased thereafter (Fig. 1 J). Because muscle γδT cells showed enhanced expression of *S1pr1* transcripts (Fig. 1 I), which encode a receptor that regulates lymphocyte egress from secondary lymphoid organs, we investigated whether accrual of γδT in injured muscle reflected migration from lymphoid tissues. Administration of the inhibitory drug FTY720, starting a day before injury, partially impaired γδT cell accumulation (Fig. 1 K). We also used the Kaede transgenic mouse system (Tomura et al., 2008) to address this point. Kaede mice ubiquitously express a photoconvertible fluorescent reporter (Kaede); exposure to violet light stably converts the reporter from green to red, facilitating tracking of cell migration across diverse sites. At the time of CTX-induced injury, we noninvasively photoconverted cells in the cervical lymph nodes. 3 d later, Kaede-red fluorescence signaled emigration of γδT cells from circulation to injured muscle, substantially more actively than to the spleen (Fig. 1 L).

Together, these data suggest that the accumulation of γδT cells in injured muscle results from a combination of local population expansion, especially at the earliest time point, and cell recruitment from lymphoid organs. Both mechanisms are consistent with our reanalysis of recently published single-cell RNA-seq (scRNA-seq) data of whole muscle isolated from mice before and 1 d after acute injury (Baht et al., 2020; Fig. S1, C–E). There was a substantial increase in cells expressing *Il1b* and *Il23a* transcripts upon injury, crucial cytokines for Tγδ17 proliferation. Additionally, cells expressing transcripts encoding chemokines

implicated in γδT cell recruitment to sites of inflammation, such as *Ccl2* and *Cxcl16*, were induced by injury. All of these transcripts were expressed mainly by *Csf1r*-expressing presumably myeloid cells, which could potentially stimulate γδT cell proliferation and recruitment.

γδT cells promote efficient muscle regeneration following injury

To address whether γδT cells influenced skeletal muscle regeneration, we punctually and cleanly depleted them before CTX-induced injury using a genetic ablation system wherein a transgene encoding the diphtheria toxin receptor (DTR) is embedded in the 3′-UTR of *Tcrd*, thereby enabling γδT cell depletion upon DT administration (Sandrock et al., 2018). After 3 d of DT treatment (Fig. 2 A), γδT cells were absent from the muscle for ≥2 wk (Fig. 2 B), which was to be expected given their restricted perinatal generation. We evaluated muscle regeneration in $DTR^{+/+}$ (which lack γδT cells) versus $DTR^{-/-}$ (which have γδT cells) littermates by both histological and transcriptional assays.

H&E staining of sections of the tibialis anterior (TA) muscle isolated 7 d after injury revealed generally similar histology in mice of the two genotypes, but there were more large multinucleated cells in animals harboring γδT cells (arrows in Fig. 2 C). Quantification of the cross-sectional areas of individual regenerating fibers, both their size distribution and average size, confirmed the increase in fiber size at the injury site of $DTR^{-/-}$ mice (Fig. 2 D), indicative of more active regeneration in the presence of γδT cells.

As an orthogonal measure of repair, we performed RNA-seq analysis on whole TA muscle at several time points after injury. *k*-means clustering of the WT time course revealed sets of transcripts that were modulated during the regenerative process in a coordinate manner. Expression of one set was weak before injury, peaked at day 3, and was turned off by day 14 (Fig. 2 E, top). This set is enriched for a wide variety of pathways related to inflammation and cell activation (Kuleshov et al., 2016). Expression of another set of transcripts showed the inverse behavior: robustly expressed before injury, turned down during active repair, and turned back up by day 14 (Fig. 2 E, bottom). This set has an abundance of transcripts encoding proteins involved in the filament structure and contractile function of muscles (Kuleshov et al., 2016). γδT cells promoted down-regulation of the inflammation/activation signature and up-regulation of the filament structure/contractile function signature at the appropriate time, as evidenced by the off-diagonal clouds on the fold-change/fold-change (FC/FC) plots of Fig. 2 F. These observations suggest that mice hosting γδT cells progressed through the regenerative process more effectively and/or more rapidly than mice without them.

γδT cells promote early inflammation and MuSC proliferation

To begin elucidating the mechanisms underlying the influence of γδT cells on skeletal muscle regeneration, we performed a broad flow cytometric analysis of cellular changes at early times after injury in littermates without versus with γδT cells. Increased Evans Blue Dye uptake indicated that mice with γδT cells displayed enhanced vascular permeability, suggesting that they might promote the early inflammatory response (Fig. 3 A). Accordingly, these mice showed significantly greater accumulation of neutrophils (Fig. 3 B), as well as a trending increase in reparative $Ly6C^{lo}$, but not inflammatory $Ly6C^{hi}$, monocyte/macrophages (MO/MFs) on day 1 after injury (Fig. 3 C). A significant, γδT cell–dependent increase in neutrophils and $Ly6C^{lo}$ MO/MFs was observed 3 d after injury, at which time the latter cell type was the dominant population of myeloid cells in the injured muscle (Fig. S2, A and B).

Given the reported effects of inflammation on MuSCs and MPCs (Tidball, 2017), and the critical dependence of muscle regeneration on MuSC proliferation and differentiation (Charge and Rudnicki, 2004; Sambasivan et al., 2011; Lepper et al., 2011), we also examined stem cells and their derivatives in DT-treated $DTR^{-/-}$ versus $DTR^{+/+}$ mice. At day 1 after injury, there was no γδT cell-dependent change in MuSC/MPC numbers (Fig. 3 D); however, muscle precursors proliferated more in the presence of γδT cells, as evidenced by greater Ki67 staining and increased 5-ethynyl-2′-deoxyuridine (EdU) uptake (Fig. 3 E). Reflecting this increase in proliferation on day 1, there were more precursors on day 3 after injury (Fig. 3 F), as well as a greater number of them in cycle ($Ki67^+$) and differentiating ($MyoG^+$; Fig. 3 G). Concordantly, whole-tissue RNA-seq on hindlimb samples collected across the time course of repair revealed more transcripts encoding the myogenic regulators, MyoG and MyoD, at early time points after injury in mice harboring γδT cells (Fig. 3 H). In addition, *Myog* transcript levels were properly down-regulated at later timepoints in mice with, but not without, γδT cells, a requirement for effective muscle regeneration.

To examine the molecular impact of γδT cells on MuSC/MPCs, we isolated them from the hindlimb at day 1 after injury from $DTR^{-/-}$ versus $DTR^{+/+}$ littermates and performed population-level RNA-seq. Gene set enrichment analysis (GSEA; Subramanian et al., 2005) revealed, as expected, a higher representation of pathways associated with growth and proliferation in the MuSCs from mice harboring γδT cells (Fig. 3 I). Taken together, these results indicate that γδT cells promoted the early stages of muscle repair after acute injury, while their absence delayed muscle regeneration and the restoration of homeostasis.

IL-17A promotes early inflammation and regeneration after acute muscle injury

To explore the molecular mechanisms used by γδT cells to promote muscle repair, we turned our attention to IL-17A, a cytokine mainly produced by muscle γδT cells in injured muscle (Fig. 1 F). IL-17A fosters tissue repair in multiple organs in response to a variety of stimuli, encompassing bacterial, chemical, and physical injury (Majumder and McGeachy, 2021). We first chose an acute loss-of-function model to assess the impact of IL-17A on MPC differentiation. We treated CTX-injured mice with neutralizing anti–IL-17A and anti–IL-17F mAbs. (The addition of anti–IL-17F mAb in this experiment was to avoid any compensatory role of IL-17F, which has been described in other contexts; Chong et al., 2020.) IL-17A/F neutralization resulted in a decrease in the $MyoG^+$ fraction of MuSC/MPCs (Fig. 4 A). We then specifically addressed the role of IL-17A in muscle repair,

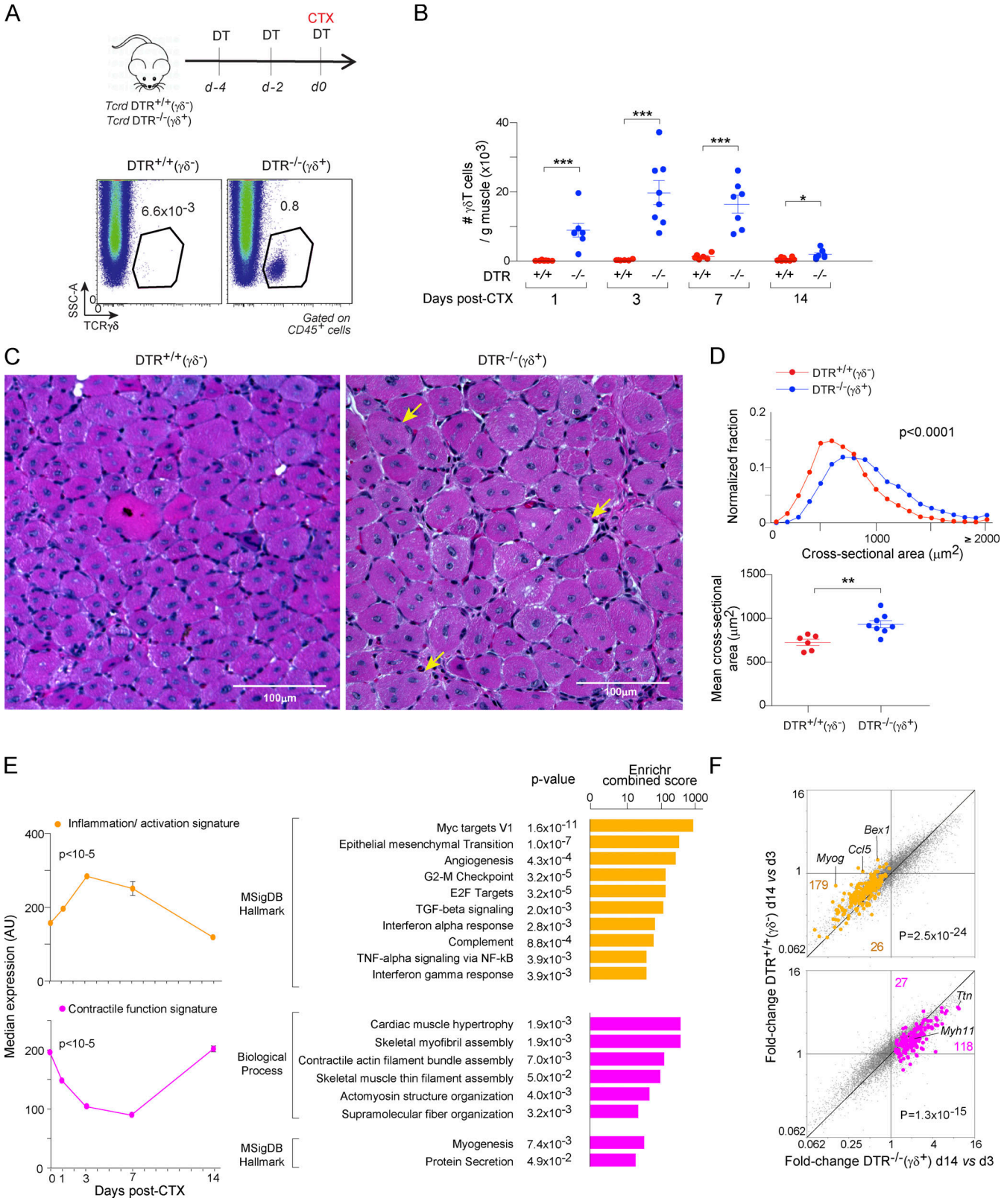

Figure 2. **γδT cells promote muscle repair. (A)** Schematic of the depletion protocol (top) and representative dot-plots of TCRγδ expression by immunocytes from muscle 3 d after injury following DT administration to littermates of the indicated genotypes (right). SSC, side scatter. **(B)** Same as A, except summary data over time after injury. Data obtained from two to three independent experiments. **(C)** H&E staining of muscle sections collected 7 d after CTX-induced injury. Arrows indicate selected examples of large multinucleated cells. Scale bar indicates 100 µm. **(D)** Cross-sectional area of muscle fibers on day 7. Top: Frequency distribution, with 100-µm^2 bins. Bottom: Mean fiber diameter per mouse. Data obtained from three independent experiments. **(E and F)** Transcriptional analysis of regenerating muscle tissue. **(E)** Gene signature scores over time for WT mice (n = 3). **(F)** FC/FC plots comparing transcriptome evolution from day 3 to 14 after injury in mice with (DTR$^{-/-}$) or without (DTR$^{+/+}$) γδT cells. Abbreviations as per Fig. 1. Means ± SEM. *, P < 0.05; **, P < 0.01; ***, P < 0.001. Statistical analyses: t test of weighted sums (D, top); otherwise unpaired t test.

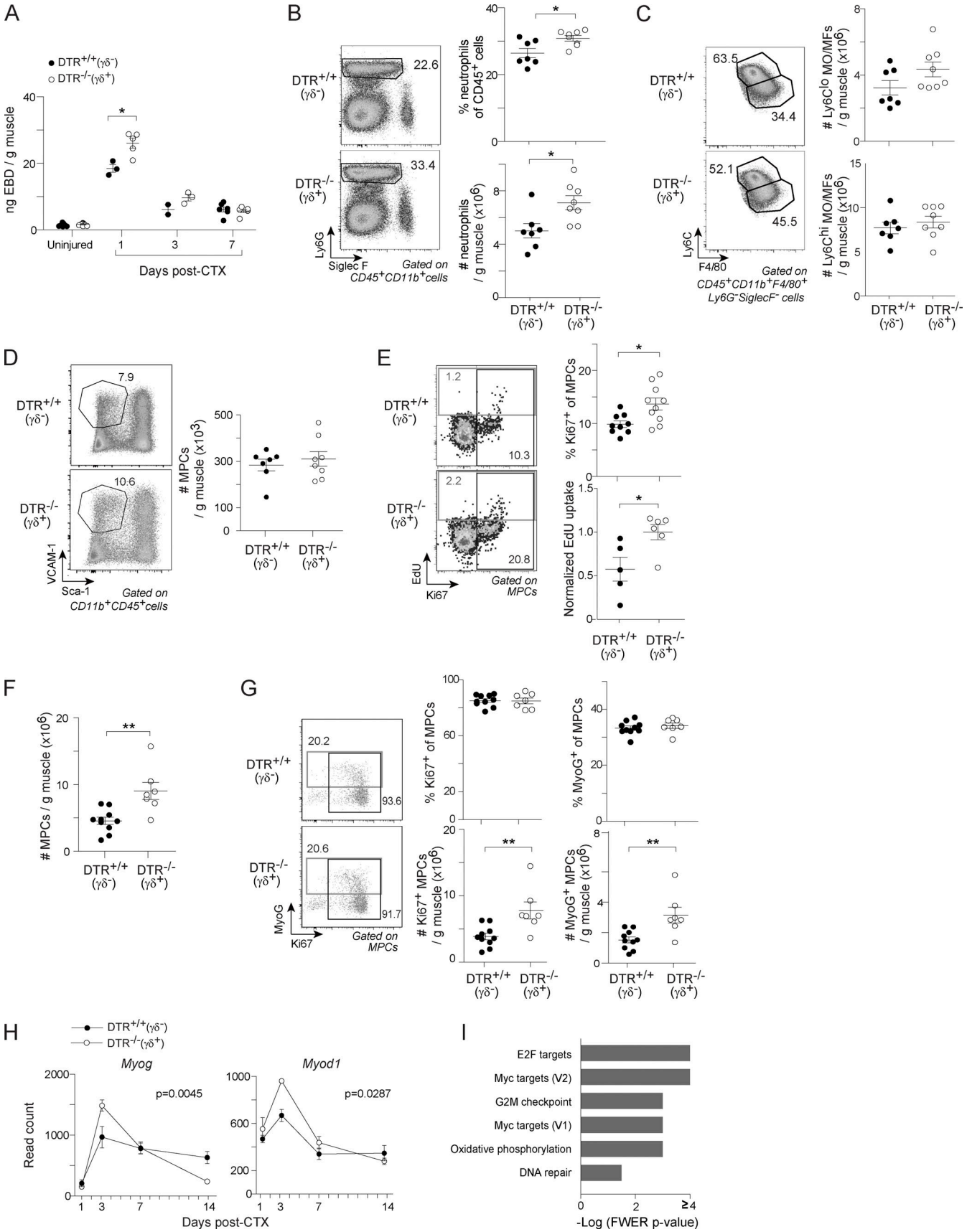

Figure 3. **γδT cells promote early inflammation and stem cell proliferation after muscle injury. (A)** Vascular permeability over time after CTX-induced injury in the TA muscle, measured by Evans blue dye uptake. Data obtained from two independent experiments. **(B)** Flow cytometric analysis of neutrophils in

day-1 injured muscle of mice harboring ($DTR^{-/-}$) or not ($DTR^{+/+}$) γδT cells. Left: Representative dot-plots. Right: Summary data for fractional representation (top) and numbers (bottom). **(C)** Same as B, except MO/MF populations were examined. **(D)** Same as B, except MPCs were examined. **(E)** Same as B, except cell-cycle state of MPCs was examined. EdU^+ fractions were normalized to the mean of the control group. **(F)** MPC numbers on day 3 after injury. **(G)** Flow cytometric analysis of Ki67 and MyoG expression by MPCs 3 d after injury of mice of the indicated genotypes. Left: Representative dot-plots. Right: Summary data/quantification. Data for B–G obtained from two to three independent experiments. **(H)** RNA-seq analysis of *Myog* and *Myod1* transcripts from whole TA muscle taken from mice with ($DTR^{-/-}$) or without ($DTR^{+/+}$) γδT cells over time after injury ($n = 3$). **(I)** GSEA of MSigDB Hallmark pathways up-regulated in MPCs isolated from $γδT^+$ ($DTR^{-/-}$) over $γδT^-$ ($DTR^{+/+}$) 1 d after injury. EBD, Evans Blue Dye; FWER, familywise error rate. Other abbreviations as per Figs. 1 and 2. Means ± SEM. *, $P < 0.05$; **, $P < 0.01$ by unpaired *t* test except for H, which used a two-way ANOVA.

because RNA-seq of sorted muscle $Vγ6^+$ cells revealed robust expression of transcripts encoding IL-17A but relatively low expression of those specifying IL-17F (Fig. S1 A). We administered rIL-17A to CTX-injured mice on days −1, 0, and 1 after injury and assessed diverse indicators of regeneration; rIL-17A was injected i.m. on day 0, along with CTX, to enhance the muscle specificity of its effects. In line with a role for γδT cells in promoting early inflammation after injury, rIL-17A supplementation resulted in greater numbers of $CD45^+$ cells in muscle on day 1 (Fig. S3 A). This increase was primarily attributable to a greater than twofold augmentation in neutrophil numbers, but also to a mild increase in $Ly6C^{lo}$ MO/MFs (Fig. 4 B). The greater numbers of neutrophils and $Ly6C^{lo}$ MO/MFs persisted in rIL-17A–treated mice on day 2 after injury (Fig. S3, B–D).

In addition to its impact on immunocytes, rIL-17A treatment promoted MuSC/MPC proliferation and muscle repair. 1 d after injury, MuSCs isolated from rIL-17A–treated mice displayed significantly enhanced EdU uptake (Fig. 4 C), and 3 d after injury, there was an increase in the absolute number and percentage of differentiated $MyoG^+$ MuSC/MPCs in rIL-17A–treated mice (Fig. 4 D). Analysis of H&E-stained sections of TA muscles removed on day 7 after CTX (Fig. 4 E) revealed that rIL-17A supplementation increased the cross-sectional area of individual muscle fibers (Fig. 4 F), a sign of more efficient repair. Whole-tissue RNA-seq of hindlimb muscles on day 7 after injury followed by data analysis using recently reported functional signatures (Aguilar et al., 2015), confirmed the pro-regenerative activity of rIL-17A. Whole-muscle transcripts from the rIL-17A–treated mice were impoverished in prerepair signatures and enriched in signatures related to restoration of homeostatic function (i.e., muscle structure and contraction), suggesting a more advanced state of regeneration (Fig. 4 G). We then two-way compared the whole-muscle transcriptomes of PBS- versus rIL-17A–treated mice vis-à-vis those of $DTR^{+/+}$ ($γδT^-$) versus $DTR^{-/-}$ ($γδT^+$) mice on day 7 after CTX. There was a clear similarity between the transcriptional profiles of regenerating muscle from rIL-17A–treated and $γδT^+$ mice. Both groups showed enrichment of a muscle homeostasis/structure signature that needs to be upregulated by day 7 to achieve homeostasis (Burzyn et al., 2013), although increase was greater for rIL-17A treatment, as indicated by the off-diagonal cloud of transcripts (Fig. 4 H). In contrast, both groups exhibited lower expression of a signature characteristic of entry into the muscle repair process, which needs to be turned down for effective continuation toward homeostasis (Burzyn et al., 2013); again, this effect was stronger for the rIL-17A–treated group (Fig. 4 H). Collectively, the data indicate that rIL-17A supplementation promoted early inflammation and enhanced muscle repair, reminiscent of the impact of γδT cells after acute injury. During revision of this paper, it was reported that neutrophils promote MuSC activation early after muscle injury (Seo et al., 2021), suggesting that at least part of the impact of γδT cells/rIL-17A on MuSC proliferation and muscle regeneration was by enhancing the recruitment of neutrophils to acutely injured muscle. Concordantly, depletion of neutrophils using anti-Ly6G antibody abrogated the pro-regenerative effect of rIL-17A at day 7 after injury, as indicated by the smaller muscle fiber cross-sectional area in mice treated with rIL-17A and anti-Ly6G compared to rIL-17A alone (Fig. S3, E and F).

Accrual of γδT cells and their enhanced IL-17A levels after muscle injury are microbiota dependent

Previous reports have identified a role for the microbiota in inducing IL-17A–producing γδT cells (Duan et al., 2010; Ismail et al., 2011; Li et al., 2017; Jin et al., 2019; Wilharm et al., 2019). A difference in muscle γδT cell numbers in mice from different vendors (Fig. S4 A) raised the question of whether the microbiota might influence γδT cell accumulation after acute skeletal muscle injury, and thereby muscle regeneration. Thus, we compared the γδT cell compartments of injured hindlimb muscles from germ-free (GF) and specific pathogen–free (SPF) animals. GF mice presented with substantially fewer muscle γδT cells day 3 after injury (Fig. 5 A). Similarly, treatment of SPF mice with a broad-spectrum antibiotic cocktail (vancomycin, metronidazole, neomycin, and ampicillin [VMNA]) resulted in a substantial drop in the representation of γδT cells (Fig. 5 B). Additionally, the γδT cells present in skeletal muscle 3 d after injury in GF and VMNA-treated mice displayed a striking reduction in Ki67 expression compared with their respective controls (Fig. 5, D and E). IL-17A production by muscle γδT cells was also significantly decreased after antibiotic treatment (Fig. 5 C), indicating a key role for the microbiota in controlling γδT cell proliferation and IL-17A production after acute injury.

To address the possibility that microbes were being introduced into skeletal muscle during the injury process (which is performed via i.m. injection through the skin), we performed a sterile surgical injury procedure wherein the skin was opened and the i.m. injection was performed without the needle passing through skin. The two procedures resulted in very similar accumulation of γδT cells in hindlimb muscle 3 d after CTX injury (Fig. S4 B).

Given that we observed a minor population of γδT cells in skeletal muscle before injury (Fig. 1, B, G, and J), and that the accumulation of γδT cells following CTX injection partially depended on egress from lymphoid organs (Fig. 1, K and L), we also analyzed the muscle and lymphoid $RORγ^+$ γδT cell

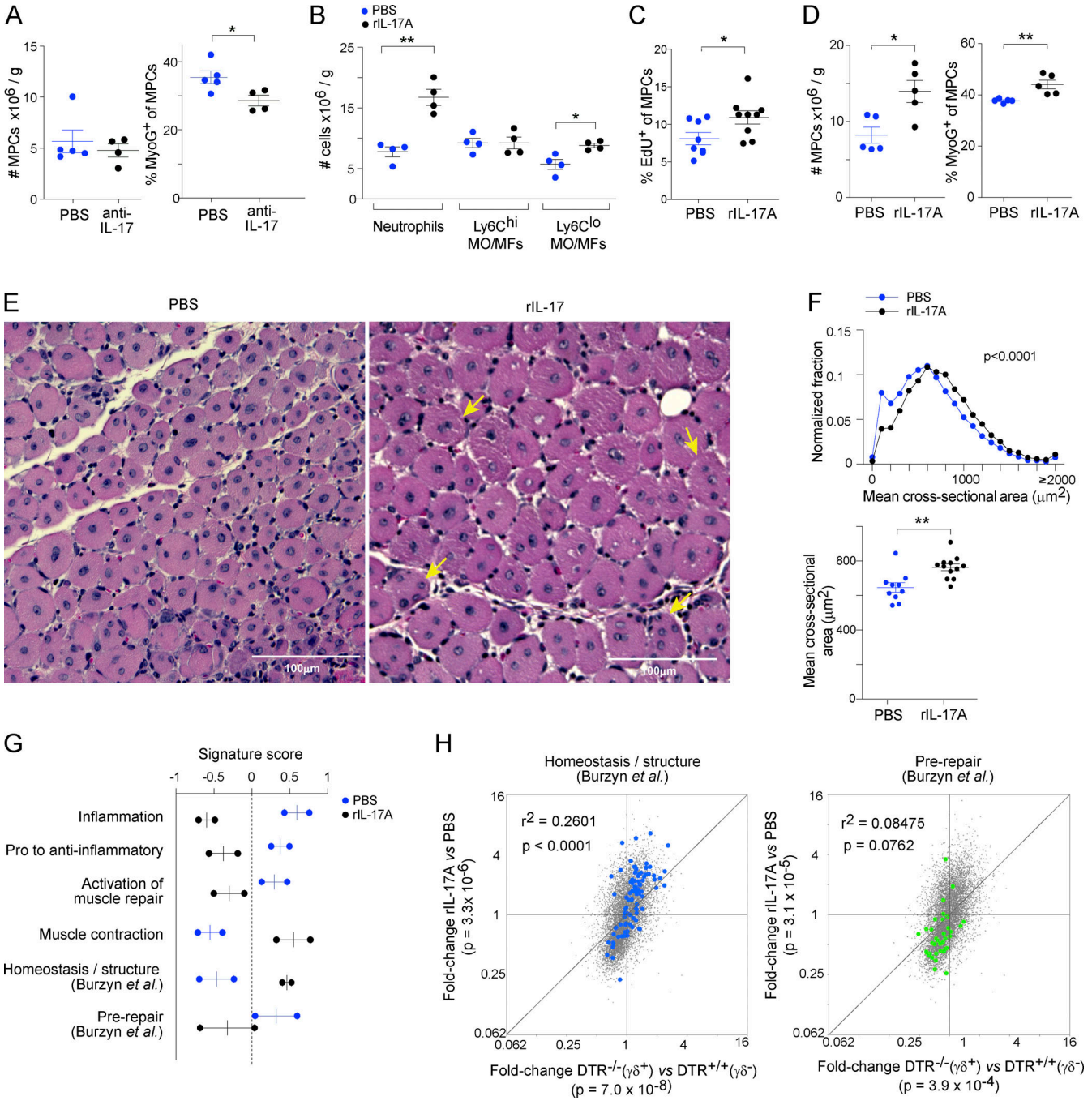

Figure 4. **IL-17A boosts early inflammation and muscle repair after acute injury. (A)** Flow cytometric quantification of total MPC number (left) and fraction (right) of MyoG$^+$ MPCs in muscle 3 d after injury with or without a combination of anti–IL-17A and anti–IL-17F (anti–IL-17) injection. Representative of two independent experiments. **(B)** Flow cytometric quantification of myeloid cell populations in hindlimb muscle of mice treated with PBS or rIL-17A 1 d after CTX. Representative of two independent experiments. **(C)** Flow cytometric analysis of EdU uptake by MPCs 1 d after CTX. Data obtained from two independent experiments. **(D)** Flow cytometric quantification of total MPC numbers (left) fraction and numbers of MyoG$^+$ MPCs muscle 3 d after injury with or without rIL-17A injection. **(E)** Histological analysis of muscle fiber regeneration 7 d after injury of mice treated with PBS or rIL-17A. Representative images of H&E staining of a hindlimb muscle section. Arrows depict large, multinucleated cells. Scale bar indicates 100 µm. **(F)** Quantification of cross-sectional areas of individual centrally nucleated muscle fibers on sections like those in E. Top: Distributions of individual fiber areas. Bottom: Average fiber areas for individual mice. Data obtained from three independent experiments. Statistical analysis of frequency distributions was performed using *t* test of weighted sums. **(G)** Gene signature scores related to various aspects of muscle regeneration (Aguilar et al., 2015) in the transcriptome of whole TA muscle on day 7 after CTX injury in the presence or absence or rIL-17A (n = 2). Score calculated as per Materials and methods. **(H)** FC/FC plots comparing gene expression values in TA muscle of mice with (DTR$^{-/-}$) versus without (DTR$^{+/+}$) γδT cells (x axis) vis-a-vis rIL-17A– versus PBS-treated mice 7 d after CTX (y axis). Muscle "homoeostasis/structure" and "entry to repair" signature genes (Burzyn et al., 2013) are highlighted in blue and green, respectively. Over- or underrepresentation of the signatures in the FC comparisons was statistically evaluated using χ^2 test. Correlations of FC values between the rIL-17A versus PBS and DTR$^{-/-}$ versus DTR$^{+/+}$ comparisons were performed using linear regression. Mean ± SEM. *, P < 0.05; **, P < 0.01 by unpaired *t* test unless otherwise indicated.

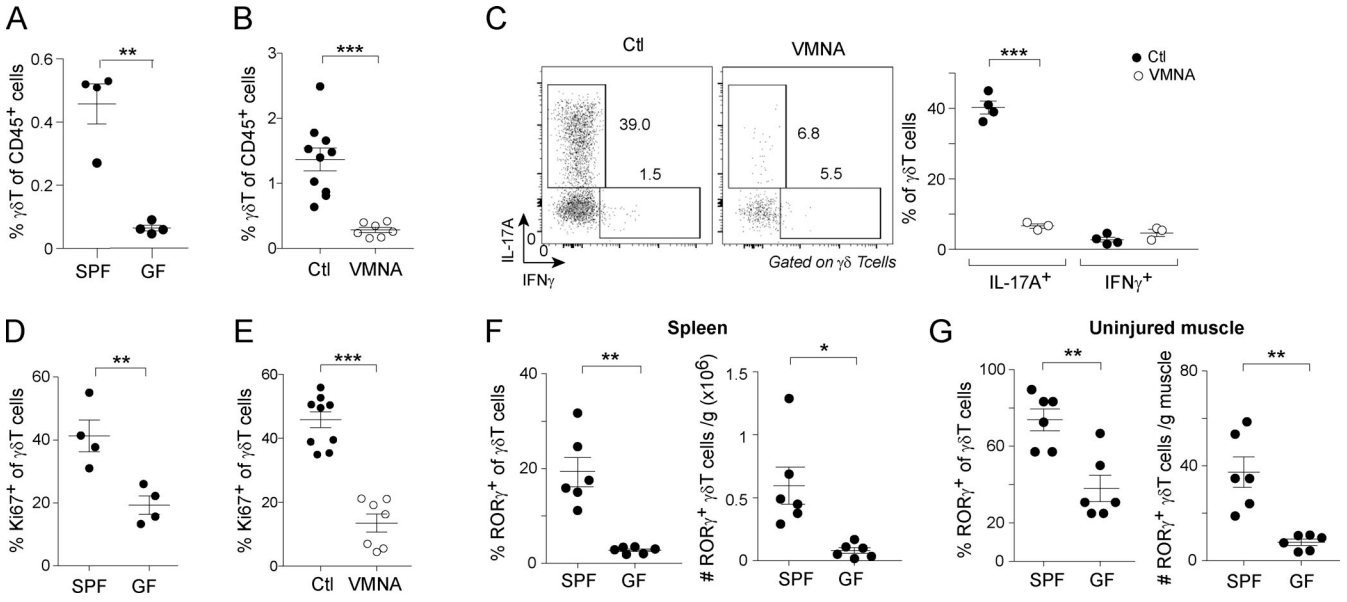

Figure 5. **The microbiota controls accumulation and IL-17A production of muscle γδT cells. (A)** Flow cytometric quantification of the fraction of γδT cells in hindlimb muscle 3 d after CTX in GF versus SPF mice. **(B)** Same as A, except SPF mice were treated or not with the antibiotic cocktail VMNA. **(C)** Flow cytometric analysis of cytokine expression by muscle γδT cells 3 d after injury. Left: Representative dot-plot. Right: Summary data. **(D)** Flow cytometric analysis of Ki67 expression by muscle γδT cells 3 d after injury in GF or SPF mice. Scale bar indicates 100 µm. **(E)** Same as D, except SPF mice were treated or not with the antibiotic cocktail VMNA. **(F)** Flow cytometric analysis of splenic RORγ⁺ γδT cells from GF or SPF mice. Left: Frequency. Right: Numbers. **(G)** Same as F, except from uninjured hindlimb skeletal muscle. A, C, and D are representative of two independent experiments; B and E–G are pooled data of two independent experiments. Mean ± SEM. *, P < 0.05; **, P < 0.01; ***, P < 0.001 by unpaired *t* test unless otherwise indicated.

compartments in SPF and GF mice that had not been injured. In both the spleen (Fig. 5 F) and uninjured hindlimb muscle (Fig. 5 G), GF mice displayed a striking reduction in the frequency and numbers of RORγ⁺ γδT cells, suggesting that the microbiota promotes the steady-state establishment and/or maintenance of RORγ⁺ γδT cell compartments in skeletal muscle as well as in lymphoid tissues. Ablation of these microbiota-dependent "progenitor" populations would subsequently impair muscle γδT cell accumulation upon injury.

The microbiota/IL-17A axis regulates muscle repair after acute injury

We wondered whether, like genetic ablation, γδT cell depletion following VMNA treatment would impair muscle regeneration, and whether this was also an IL-17A–dependent process. On day 1 after injury, VMNA-treated mice failed to launch an efficient inflammatory response in the injured muscle, as evidenced by the lower numbers of CD45⁺ cells in the muscle (Fig. 6 A). This drop was observed for all major myeloid cell types, including neutrophils and Ly6C^{hi} and Ly6C^{lo} MO/MFs (Fig. 6 B). In addition to its impact on immunocytes, VMNA treatment reduced the numbers of MuSC/MPCs (Fig. 6 C). Supplementation of VMNA-treated mice with rIL-17A was able to restore the number of muscle CD45⁺ cells to control levels, which was primarily driven by enhanced neutrophil accumulation (Fig. 6, A and B).

In line with its impact on γδT cell proliferation and the early inflammatory response after injury, VMNA treatment resulted in a considerable delay in muscle repair according to multiple criteria. First, VMNA-treated mice had a larger immunocyte infiltrate day 7 after injury, indicative of poor resolution of inflammation (Fig. S5, A–C). In addition, histological analysis showed VMNA treatment to result in smaller muscle-fiber sizes at day 7 after injury (Fig. 6, D and E). We also observed more muscle fibrosis, a consequence of poor repair, in the VMNA group (Fig. 6 F). rIL-17 supplementation of VMNA-treated mice partially restored effective muscle regeneration at day 7 after injury, as evidenced by a drop in myeloid cell numbers (Fig. S5, A–C), increased muscle-fiber size (Fig. 6, D and E), and decreased collagen deposition (Fig. 6 F) compared with the VMNA-alone group. Thus, in three experimental contexts—different mouse vendors, GF versus SPF mice, and antibiotic- versus control-injected mice—the accumulation of IL-17⁺ γδT cells in injured skeletal muscle was microbiota-dependent. There were defects in muscle inflammation and regeneration in antibiotic-treated mice, which could be complemented by administration of rIL-17A.

Discussion

Muscle regeneration is a dynamic multistep process that is tightly coordinated by various inflammatory signals from diverse immunocyte types. Past research has established a role for the inflammatory response in initiating early stages of repair. In the current study, we identified a previously unreported population of IL-17A⁺ γδT cells that accumulated at early stages of muscle injury, resulting in heightened inflammation and accelerated tissue repair. The accrual of IL-17A⁺ RORγ⁺ γδT cells in this acute inflammatory context contrasts with a published report on the *mdx* mouse model of chronic injury associated with muscular dystrophy (Cascabulho et al., 2016). In *mdx* mice,

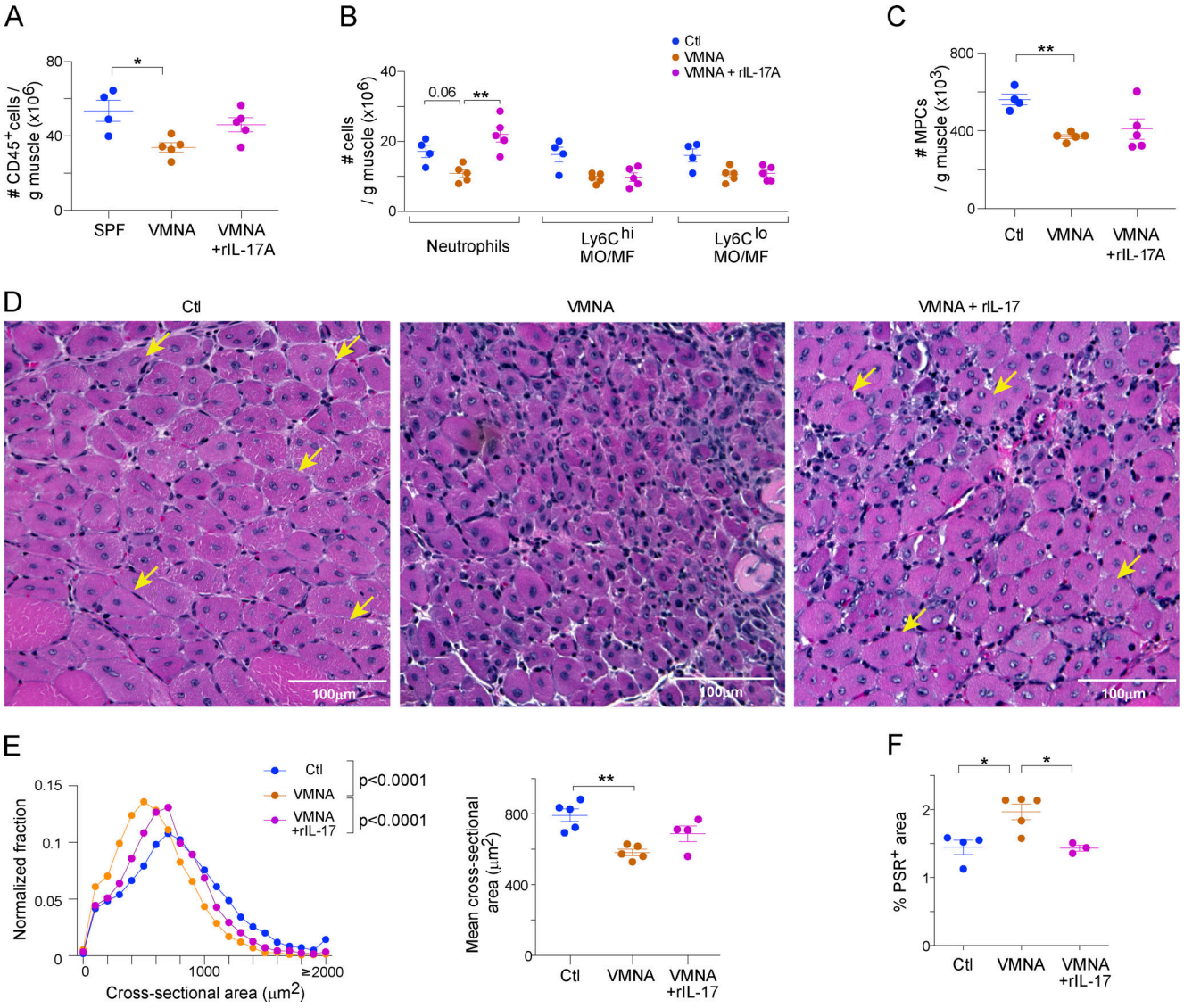

Figure 6. **The microbiota controls muscle repair. (A–C)** Flow cytometric quantification of total immunocytes (A), myeloid cell populations (B), and MPCs (C) in hindlimb muscle 1 d after injury. **(D)** Representative images of H&E staining of hindlimb muscle 7 d after injury in conjunction with VMNA treatment ± a combination of rIL-17A and rIL-17F (rIL-17). Arrows indicate selected examples of large multinucleated cells. **(E)** Quantification of cross-sectional areas of individual centrally nucleated muscle fibers on H&E sections per panel (D). Left: Distribution of individual fibers area control (Ctl; SPF mice, PBS treated) versus VMNA and VMNA versus VMNA + rIL-17 comparisons via *t* test of weighted sums. Right: Average fiber areas for individual mice. **(F)** Quantification of muscle fibrotic area 7 d after injury using picrosirius red (PSR) staining. Results from three to five independent mice. Means ± SEM. *, P < 0.05; **, P < 0.01 using unpaired *t* test unless otherwise indicated. When three groups were analyzed, one-way ANOVA with Bonferroni post hoc test was performed.

IFN-γ–producing, but not IL-17A–producing, γδT cells accumulated in inflamed cardiac muscle, suggesting that the nature of γδT cell accumulation in damaged muscle can vary with the mode of muscle damage and/or the type of muscle involved (i.e., acute versus chronic, skeletal versus cardiac). Another report described muscle-infiltrating γδT cells that produced GM-CSF in response to immunization with myosin in complete Freund's adjuvant (Kageyama et al., 2017). Although this finding supports the idea that γδT cells can accumulate in muscle, the mode of muscle damage is very different from acute CTX-induced injury, and our transcriptional analysis did not show any detectable expression of *Csf2* in the muscle γδT cell population in CTX-injured mice.

It is likely that much of the pro-reparative activity of muscle IL-17A$^+$ γδT cells is mediated through enhancement of neutrophil accumulation after injury. Neutrophils are the earliest cell type to infiltrate damaged muscle, and they play a key role in clearing necrotic muscle fibers, a crucial step in mobilizing the repair machinery (Teixeira et al., 2003; Nishimura et al., 2015). Neutrophil recruitment was one of the earliest roles attributed to IL-17A, and this function has been observed in a variety of tissues (Ye et al., 2001; Laan et al., 1999; Hoshino et al., 1999; Witowski et al., 2000). Yet, this cytokine has not to date been implicated in skeletal muscle regeneration. Failure to effectively expand the neutrophil, and eventually the MO/MF, populations at the injury site was associated with inefficient MuSC

proliferation and differentiation and the deterioration of muscle regeneration. While the increased MuSC/MPC numbers in γδT⁺ and rIL-17A–treated mice might be a consequence of their more potent inflammatory response, our data are also compatible with a direct impact of IL-17a on progenitor cells, especially given their substantial expression of *Il17ra* and *Il17rc* by these cells. Studies in various tissues, in contexts of both wound healing and tumorigenesis, have demonstrated a role for IL-17A in promoting the proliferation of stem/progenitor cell populations (Zhao et al., 2020; Chen et al., 2019; Wu et al., 2015; Zepp et al., 2017; Huang et al., 2009), so it is quite plausible that IL-17A does directly promote MuSC proliferation independent of its role in driving inflammation and neutrophil recruitment.

We further demonstrated an intriguing role of the microbiota in promoting muscle regeneration. Since rIL-17A supplementation complemented some of the regenerative defects in mice with a compromised gut microbiota, and γδT cells were the major IL-17A–producing cells in injured muscle, it is likely that the microbiota exerted its pro-regenerative effect through augmentation of early inflammation via IL-17A⁺ γδT cells. Previous reports have argued for a role for the microbiota in regulating muscle mass by modulating myocyte metabolic function (Lahiri et al., 2019). Microbiota control of muscle IL-17A⁺ γδT cells constitutes a previously unidentified mode by which microbial signals can impact muscle health in response to injury. Our reanalysis of published scRNA-seq data from healthy human skeletal muscle (De Micheli et al., 2020) revealed the presence of γδT cells, suggesting the possibility of a similar axis in humans. These findings enrich our understanding of the contribution of immunocytes to muscle repair under physiologic conditions, and potentially in contexts of chronic muscle diseases such as muscle wasting, infection, dystrophy, and inflammation.

Materials and methods

Mice

C57BL/6J mice were purchased from Jackson Laboratory or Taconic Biosciences. Unless specifically noted (such as comparing mice between difference facilities), controls and treated mice were always obtained from the same facility, either freshly arrived from JAX or bred in-house. The Kaede tg mouse line (Tomura et al., 2008) was obtained from Dr O. Kanagawa (Riken, Wako, Japan). $Tcrd^{GDL}$ (GFP-DTR-luciferase), referred to here as $Tcrd^{DTR}$ mice, were previously described (Sandrock et al., 2018). Littermate mice from heterozygote crosses were used for all $Tcrd^{DTR}$ experiments. 6–10-wk-old male and female mice were used for all experiments. All mice were housed in our SPF facility at Harvard Medical School. All experiments were conducted under protocols approved by Harvard Medical School's Institutional Animal Care and Use Committee.

For CTX-induced muscle injury, mice were anesthetized with i.p. administration of ketamine:xylazine in combination (10: 2 mg/kg) and injected with 0.03 ml per muscle of *Naja mossambica* CTX (0.03 mg/ml; Sigma-Aldrich) in one or more hindlimb muscles (TA, gastrocnemius, and quadriceps), as previously described (Burzyn et al., 2013). To block egress of lymphocytes from peripheral organs, we i.p. injected mice with 1 mg/kg FTY720 (Cayman Chemical) 1 d before injury and daily thereafter. $Tcrd^{DTR+/+}$ and $Tcrd^{DTR-/-}$ male littermates were i.p. injected with DT (D0564; Sigma-Aldrich) in PBS at 15 ng/g on days −4, −2, and day of injury. For in vivo IL-17 neutralization, mice were i.p. injected with a combination of 200 µg anti–IL-17A (clone 17F3) and 200 µg anti–IL-17F (clone MM17F8F5.1A9). On the day of injury, a combination of anti–IL-17A and anti–IL-17F (50 µg/muscle) was injected intramuscularly along with CTX. Control mice were injected with the equivalent amount of IgG1 isotype (clone MOPC-21). For neutrophil depletion, mice were i.p.-injected with 200 µg anti-Ly6G (clone 1A8) or the corresponding IgG2a isotype control (clone 2A3) on day −1 and the day of injury. All in vivo antibodies were purchased from BioXcell. For in vivo rIL-17 administration, 500 ng of rIL-17A or a combination of 500 ng rIL-17A and 500 ng rIL-17F (Peprotech) was i.p.-injected into mice in sterile PBS on the day before and the day after injury. On the day of injury, rIL-17A or a combination of rIL-17A and rIL-17F (0.1 µg/muscle) was injected intramuscularly along with CTX. For antibiotic treatment, mice were administered 0.5 mg/ml vancomycin (RPI), 1 mg/ml metronidazole (Sigma-Aldrich), 1 mg/ml neomycin (Thermo Fisher Scientific), and 1 mg/ml ampicillin (Sigma-Aldrich; VMNA) dissolved in drinking water for 3 wk before muscle injury.

Flow cytometry

The following antibodies were used for flow cytometric staining: anti-CD3 (145-2C11), anti-TCRγδ (GL3), anti-TCRβ (H57-597), anti-CD4 (GK1.5), anti-CD8a (53-5.8), anti-CD45 (30-F11), anti-CD11b (M1/70), anti-F4/80 (BM8), anti-Ly6C (HK1.4), anti-Ly6G (1A8), anti–IL-17A (TC11-18H10.1), anti–IFN-γ (XMG1.2), anti-Vγ4 (Vγ2 in alternate nomenclature; anti–UC3-10A6), anti-CD31 (390), anti–Sca-1 (Ly6A/E; D7), and anti–VCAM-1 (CD106; M/K-2), all from BioLegend; anti-Siglec F (E50-2440) from eBioscience; and anti-MyoG (F5D) and anti-Ki67 (B56) from BD Pharmingen. Staining for Vγ6 was performed using the 17D1 hybridoma, kindly provided by Drs. Bob Tigelaar and Julia Lewis (Yale University Medical School, New Haven, CT), after staining with anti-Cδ mAb, GL3 (Roark et al., 2004). Goat anti-rat IgM from Jackson ImmunoResearch Laboratories was used to detect 17D1 staining. Surface staining was performed for 30 min at 4°C, and viability was assessed using Invitrogen LIVE/DEAD Fixable viability dye as per the manufacturer's instructions. Intracellular staining was performed using eBiosciences Intracellular Fixation & Permeabilization buffer set. For ex vivo intracellular cytokine staining, single-cell suspensions were stimulated for 3.5 h at 37°C with 50 ng/ml PMA and 1 µM ionomycin (both Sigma-Aldrich) in the presence of protein transport inhibitor cocktail (eBioscience) in complete RPMI 1640 supplemented with 10% FBS (Thermo Fisher Scientific). For in vivo proliferation experiments, 1 mg EdU (Thermo Fisher Scientific) was administered i.p. 4 h before analysis. Staining was performed using Pacific Blue–coupled azide following the manufacturer's instructions. Cells were acquired with an LSRII or FACSymphony flow cytometer (both BD Biosciences). Data were analyzed using FlowJo software (TreeStar).

Cell isolations

Isolation of lymphocytes was done as previously described (Burzyn et al., 2013). Briefly, hindlimb muscles were excised, minced, and digested at 37°C for 30 min in a solution containing DMEM (2% FCS, collagenase II [2 mg/ml; Thermo Fisher Scientific], and DNase I [100 µg/ml; Sigma-Aldrich]). Leukocytes were enriched by Percoll (GE Healthcare) density centrifugation (40%:80%, 25 min at 1,126 *g*). The interphase containing leukocytes was recovered, washed, and stained for analysis or sorting by flow cytometry. Isolation of muscle MuSCs/MPCs and myeloid cells was done as previously described (Liu et al., 2015). Briefly, hindlimb muscles were minced and digested by collagenase II (800 U/ml) in Ham's F10 with 10% horse serum at 37°C for 90 min, followed by a second digestion step using collagenase II (80 U/ml) and dispase (1 U/ml) for 30 min. Cell suspensions were passed through a 20-gauge needle 10 times and then filtered through a 40-µm cell strainer, washed, and stained for analysis or sorting by flow cytometry. Intestinal tissues were cleaned and treated with RPMI 1640 containing 1 mM DTT, 20 mM EDTA, and 2% FBS at 37°C for 15 min to remove epithelial cells, minced, and dissociated in collagenase solution (1 mg/ml collagenase 8 and 0.05 mg/ml DNaseI, both from Sigma-Aldrich, and 1% FCS in RPMI 1640) with constant stirring at 37°C for 20 min. Single-cell suspensions were filtered and washed with 10% FCS RPMI 1640 solution before staining and sorting by flow cytometry.

TCR sequence analysis

Vγ6$^+$ T cells (Vγ6$^+$ TCRγδ$^+$ CD45$^+$ TCRβ$^-$ CD19$^-$ DAPI$^-$) were individually sorted into wells in a 96-well plate containing 10 µl reverse transcription buffer containing 5× first strand buffer, MMLV-RT, RNaseOUT, and oligo-dT, all from Invitrogen. Additionally, the buffer included 0.5 mM DTT, 0.02% Triton X-100, and 0.01% BSA. Following sorting, the wells were overlaid with mineral oil and placed in an incubator at 37°C for 3 h to generate cDNAs. After cDNA generation, two rounds of nested PCR using primers (Paget et al., 2015) targeting the VDJ junction of *Trdv4* were used to generate products for Sanger sequencing. TRDV4external: 5′-CTTCTACTGCACTGTAACAGGAG-3′; TRDV 4internal: 5′-CTCGACATTCAGAAGGCAACA-3′; TRDCexternal: 5′-GCACTGTACTTCCCGCTGG-3′; TRDCinternal: 5′-ATCTTTCA CCAGACAAGCAACA-3′. Aliquots of the final PCR products were visualized on a 2% agarose gel to identify wells with successful amplification. Those products were treated with ExoSAP-IT (Thermo Fisher Scientific) and then underwent Sanger sequencing using the TRDCinternal primer at the Dana-Farber/Harvard Cancer Center High-Throughput Sequencing Core. Raw reads were filtered for quality and then parsed using IMGT/V-QUEST. Sequences that did not result in a productive TCR rearrangement were not included in further analysis.

RNA-seq library preparation, sequencing, and data processing

Cells were double-sorted by Moflo into TCL buffer (Qiagen) containing 1% 2-mercaptoethanol (Sigma-Aldrich), libraries were constructed and sequenced, and the data were processed according to the Immgen protocol (https://www.immgen.org/img/Protocols/ImmGenULI_RNAseq_methods.pdf). The Smart-seq2 protocol was used for library construction (Picelli et al., 2013; Picelli et al., 2014), and RNAClean XP beads (Beckman Coulter) were used to capture and purify RNA. An anchored oligo(dT) primer (5′–AAGCAGTGGTATCAACGCAGAGTACT30 VN-3′) was used to select poly-A mRNA, which was subsequently reverse-transcribed to cDNA and PCR amplified. The Nextera XT DNA Library Preparation Kit (Illumina) was used to perform Tn5 transposon-based fragmentation. Barcoded primers were used in another round of PCR amplification (12 cycles) to introduce unique combinations of Illumina P5 and P7 barcodes to different samples, enabling pooling of samples before sequencing. Sequencing was performed on an Illumina NextSeq500 (two full NextSeq runs per batch of 96 samples, for 10M raw reads/sample on average) using 2× 38-bp reads with no further trimming. STAR 2.7.3a was used to align the sequencing reads to the mouse genome (GENCODE GRCm38/mm10 primary assembly and gene annotations vM25). Transcripts annotated as ribosomal RNA were removed. Quantification at the gene level was calculated using the Subread 2.0 command featureCounts. Subsequent normalization of raw read counts was performed in the Bioconductor package DESeq2 using the median of ratios method. Samples with <1 million reads were excluded from normalization. After normalization, GCT and CLS files were generated and used for downstream analysis. After normalization, reads were further filtered by minimal expression and coefficient of variation in Multiplot Studio (GenePattern; Broad Institute).

For whole-muscle RNA-seq library construction, total RNAs were isolated from TA muscles using TRIzol (Invitrogen) according to the manufacturer's instructions. 2 ng RNA were suspended in 5 µl TCL + 1% 2-mercaptoethanol and used for generating libraries, as described above for sorted cells.

Analysis of transcriptional data

Gene expression dynamics of whole muscles removed from WT mice over time after injury were assessed using a two-step regression modeling strategy implemented with maSigPro (Nueda et al., 2014). An α of 0.05 was used to account for multiple hypothesis testing, and a false discovery rate of 5% was applied to first identify differentially expressed transcripts. To identify coexpression clusters (or modules) during the time series, silhouette analysis partitioned differential genes into five clusters (cluster correlation, $r^2 > 0.65$). Enrichr (Kuleshov et al., 2016) was used to perform pathway analysis on cluster gene lists. For gene signature scoring, the normalized gene expression matrix was log-transformed, and the z-score of each gene was calculated. This matrix was used to calculate gene expression scores for each module using the score_genes function in the scanpy package in Python. The annotated list of gene modules was obtained from previously published studies that identified transcriptional changes during muscle injury (Burzyn et al., 2013; Aguilar et al., 2015). Volcano and FC/FC plots were generated using Multiplot Studio. Analysis of differentially expressed genes between classes of samples was performed with GSEA (Subramanian et al., 2005), using the Hallmark gene sets.

Analysis of cell migration via the Kaede system

Kaede mice were anesthetized with ketamine:xylazine in combination (10:2 mg/kg i.p.). Photoconversion of the central LNs

was done as previously described (Morton et al., 2014). Briefly, the fur attached to the skin covering the cervical region was removed using depilatory cream applied for 3 min. Violet light (Electra Pro Series 405 nm Violet Handheld Laser; Laserglow Technologies) was shone on the exposed area for 5 mins. Hindlimb muscles were injured with CTX, and the fractions of Kaede-red cells in various immunocyte populations were analyzed by flow cytometry after 72 h.

scRNA-seq analysis

Whole-muscle scRNA-seq data from days 0 and 1 after acute injury (Baht et al., 2020) was used to quantify the expression of *Il1b* and *Il23a* in various cell types. Data analysis was done using the Seurat package (Hao et al., 2021). Cells with <1,000 genes, >20,000 unique molecular identifiers, or >0.07% of reads mapped to mitochondrial genes were excluded from the analysis. Data were normalized using the NormalizeData function and scaled using the ScaleData function. Variable genes were found by the FindVariableGenes function. Principal components were calculated using the RunPCA function. Clustering was done on the top 20 principal components using FindNeighbors and FindClusters functions followed by Uniform Manifold Approximation and Projection (UMAP) dimensionality reduction using the RunUMAP function. Visualization of transcript density or signature scores was done via the Nebulosa package (Alquicira-Hernandez and Powell, 2021).

Evans blue dye uptake assay

Evans Blue Dye extravasation into skeletal muscle was measured to assess vascular permeability at different times after injury (Radu and Chernoff, 2013). In brief, 1% wt/vol sterile filtered Evans Blue Dye (EBD) was i.p. injected into mice 24 h before tissue harvest, at 1% volume to bodyweight. TA muscles were collected and incubated overnight at 55°C in 100% formamide to extract EBD into solution. EBD concentration in solution was evaluated by measuring the absorbance at 620 nm. A standard curve was used to derive the absolute mass of EBD extract from the tissue, which was then normalized to the mass of the tissue.

Histology

Injured TA muscles were collected and fixed in 10% formalin. Tissues were processed at the Rodent Histopathology Core at Harvard Medical School for H&E (for fiber size analysis) and picrosirius red (for fibrosis) staining. Four sections, 200 µm apart, were recovered and stained for analysis. Images were acquired with a Nikon Ti inverted microscope. We analyzed repair histologically as previously described (Almada et al., 2021; Kuswanto et al., 2016). In brief, we first identified the section from each sample with the largest number of regenerating muscle fibers (centrally nucleated fibers). For four to five representative regions in each of these sections, the cross-sectional area of individual muscle fibers was calculated by manually tracing the fiber circumference in Fiji (Schindelin et al., 2012). Approximately 1,000 fibers were traced per sample. To assess fibrosis, the fraction of Picrosirius Red–stained area in TA muscle sections was determined using ImageJ 1.53c.

Statistical analyses

All statistical analyses were performed using GraphPad Prism software. If not stated otherwise, data are presented as mean ± SEM. Statistical significance was calculated by unpaired Student's *t* test (two-tailed), *t* test of weighted sums, one-way ANOVA, or two-way ANOVA. $P < 0.05$ was considered significant. P values for gene signature enrichment either up or down between a pairwise comparison in volcano plots and FC/FC plots were determined using the χ^2 test.

Online supplemental material

Fig. S1 shows expanded analysis of gene expression by Vγ6$^+$ T cells and scRNA-seq from whole muscle before and after injury. Fig. S2 shows profiling of myeloid cell populations 3 d after injury in the context of γδT cell depletion. Fig. S3 shows the impact of rIL-17A supplementation on myeloid cell populations at different times as well as the impact of neutrophil depletion on repair in the context of rIL-17A supplementation. Fig. S4 shows the frequency of γδT cells in injured muscle of mice obtained from different facilities and the impact of the method of injury on γδT cell accumulation in injured muscle 3 d after injury. Fig. S5 shows the impact of antibiotic and rIL-17 treatment on various immunocyte populations 7 d after injury.

Data availability

RNA-seq data comparing Vγ6$^+$ T cells from injured muscle and the colonic lamina propria, whole-tissue RNA samples from a time course after repair in DTR$^{-/-}$ versus DTR$^{+/+}$ mice, whole-tissue RNA samples from 7 d after injury in JAX mice treated with either PBS or rIL-17A, and sorted MuSCs/MPCs from either DTR$^{-/-}$ or DTR$^{+/+}$ mice 1 d after injury have been deposited to Gene Expression Omnibus database under accession number GSE190588.

Acknowledgments

We thank R. Tigelaar and J. Lewis of Yale University Medical School for the 17D1 hybridoma; K. Hattori, N. Asinovski, A. Ortiz-Lopez, F. Chen, A. Baysoy, L. Yang, O. Yaghi, P.K. Langston, R. Ramirez, and G. Wang for experimental assistance; C. Laplace for assistance with graphics; R. Stephansky for microscopy assistance; the Harvard Medical School (HMS) Rodent Histopathology Core; and the HMS Immunology Department Flow-Cytometry Core.

This work was funded by grants from the National Institutes of Health (R01 AR070334) and the JPB Foundation to D. Mathis. B.S. Hanna was supported by a Deutsche Forschungsgemeinschaft fellowship (HA 8510/1).

Author contributions: A.O. Mann, B.S. Hanna, and D. Mathis designed experiments. A.O. Mann, B.S. Hanna, and A.M. Muñoz-Rojas performed experiments and analyzed data. I. Sandrock and I. Prinz provided the *Tcrd*^{DTR} mice. D. Mathis and C. Benoist provided supervision. A.O. Mann, B.S. Hanna, and D. Mathis wrote the manuscript, which all authors reviewed. D. Mathis furnished funding.

Disclosures: The authors declare no competing financial interests.

Submitted: 14 July 2021
Revised: 23 February 2022
Accepted: 16 March 2022

References

Aguilar, C.A., A. Shcherbina, D.O. Ricke, R. Pop, C.T. Carrigan, C.A. Gifford, M.L. Urso, M.A. Kottke, and A. Meissner. 2015. In vivo monitoring of transcriptional dynamics after lower-limb muscle injury enables quantitative classification of healing. *Sci. Rep.* 5:13885. https://doi.org/10.1038/srep13885

Akitsu, A., H. Ishigame, S. Kakuta, S.H. Chung, S. Ikeda, K. Shimizu, S. Kubo, Y. Liu, M. Umemura, G. Matsuzaki, et al. 2015. IL-1 receptor antagonist-deficient mice develop autoimmune arthritis due to intrinsic activation of IL-17-producing CCR2$^+$Vγ6$^+$γδ T cells. *Nat. Commun.* 6:7464. https://doi.org/10.1038/ncomms8464

Almada, A.E., N. Horwitz, F.D. Price, A.E. Gonzalez, M. Ko, O.V. Bolukbasi, K.A. Messemer, S. Chen, M. Sinha, L.L. Rubin, et al. 2021. FOS licenses early events in stem cell activation driving skeletal muscle regeneration. *Cell Rep.* 34:108656. https://doi.org/10.1016/j.celrep.2020.108656

Alquicira-Hernandez, J., and J.E. Powell. 2021. Nebulosa recovers single cell gene expression signals by kernel density estimation. *Bioinformatics*. https://doi.org/10.1093/bioinformatics/btab003

Alves de Lima, K., J. Rustenhoven, S. Da Mesquita, M. Wall, A.F. Salvador, I. Smirnov, G.M. Cebinelli, T. Mamuladze, W. Baker, Z. Papadopoulos, et al. 2020. Meningeal γδ T cells regulate anxiety-like behavior via IL-17a signaling in neurons. *Nat. Immunol.* 21:1421–1429. https://doi.org/10.1038/s41590-020s4150776-4

Arnold, L., A. Henry, F. Poron, Y. Baba-Amer, N. van Rooijen, A. Plonquet, R.K. Gherardi, and B. Chazaud. 2007. Inflammatory monocytes recruited after skeletal muscle injury switch into antiinflammatory macrophages to support myogenesis. *J. Exp. Med.* 204:1057–1069. https://doi.org/10.1084/jem.20070075

Baht, G.S., A. Bareja, D.E. Lee, R.R. Rao, R. Huang, J.L. Huebner, D.B. Bartlett, C.R. Hart, J.R. Gibson, I.R. Lanza, et al. 2020. Meteorin-like facilitates skeletal muscle repair through a Stat3/IGF-1 mechanism. *Nat. Metab.* 2: 278–289. https://doi.org/10.1038/s42255-020-0184-y

Barros-Martins, J., N. Schmolka, D. Fontinha, M. Pires de Miranda, J.P. Simas, I. Brok, C. Ferreira, M. Veldhoen, B. Silva-Santos, and K. Serre. 2016. Effector γδ T cell differentiation relies on master but not auxiliary Th cell transcription factors. *J. Immunol.* 196:3642–3652. https://doi.org/10.4049/jimmunol.1501921

Burzyn, D., W. Kuswanto, D. Kolodin, J.L. Shadrach, M. Cerletti, Y. Jang, E. Sefik, T.G. Tan, A.J. Wagers, C. Benoist, et al. 2013. A special population of regulatory T cells potentiates muscle repair. *Cell.* 155:1282–1295. https://doi.org/10.1016/j.cell.2013.10.054

Cascabulho, C.M., D.G. Beghini, M. Meuser-Batista, C. Penido, and A. Henriques-Pons. 2016. Chemotaxis and immunoregulatory function of cardiac γδ T cells in dystrophin-deficient mice. *J. Immunol.* 197:3531–3544. https://doi.org/10.4049/jimmunol.1600335

Castiglioni, A., G. Corna, E. Rigamonti, V. Basso, M. Vezzoli, A. Monno, A.E. Almada, A. Mondino, A.J. Wagers, A.A. Manfredi, et al. 2015. FOXP3$^+$ T cells recruited to sites of sterile skeletal muscle injury regulate the fate of satellite cells and guide effective tissue regeneration. *PLoS One.* 10. e0128094. https://doi.org/10.1371/journal.pone.0128094

Charge, S.B., and M.A. Rudnicki. 2004. Cellular and molecular regulation of muscle regeneration. *Physiol. Rev.* 84:209–238. https://doi.org/10.1152/physrev.00019.2003

Chen, S.E., B. Jin, and Y.P. Li. 2007. TNF-alpha regulates myogenesis and muscle regeneration by activating p38 MAPK. *Am. J. Physiol. Cell Physiol.* 292:C1660–C1671. https://doi.org/10.1152/ajpcell.00486.2006

Chen, X., G. Cai, C. Liu, J. Zhao, C. Gu, L. Wu, T.A. Hamilton, C.J. Zhang, J. Ko, L. Zhu, et al. 2019. IL-17R-EGFR axis links wound healing to tumorigenesis in Lrig1$^+$ stem cells. *J. Exp. Med.* 216:195–214. https://doi.org/10.1084/jem.20171849

Cheng, M., M.H. Nguyen, G. Fantuzzi, and T.J. Koh. 2008. Endogenous interferon-gamma is required for efficient skeletal muscle regeneration. *Am. J. Physiol. Cell Physiol.* 294:C1183–C1191. https://doi.org/10.1152/ajpcell.00568.2007

Chien, Y.H., C. Meyer, and M. Bonneville. 2014. γδ T cells: first line of defense and beyond. *Annu. Rev. Immunol.* 32:121–155. https://doi.org/10.1146/annurev-immunolan032713-120216

Chong, W.P., M.J. Mattapallil, K. Raychaudhuri, S.J. Bing, S. Wu, Y. Zhong, W. Wang, Z. Chen, P.B. Silver, Y. Jittayasothorn, et al. 2020. The cytokine IL-17A limits Th17 pathogenicity via a negative feedback loop driven by autocrine induction of IL-24. *Immunity.* 53:384–397. https://doi.org/10.1016/j.immuni.2020.06.022

Cua, D.J., and C.M. Tato. 2010. Innate IL-17-producing cells: the sentinels of the immune system. *Nat. Rev. Immunol.* 10:479–489. https://doi.org/10.1038/nri2800

De Micheli, A.J., J.A. Spector, O. Elemento, and B.D. Cosgrove. 2020. A reference single-cell transcriptomic atlas of human skeletal muscle tissue reveals bifurcated muscle stem cell populations. *Skelet. Muscle.* 10:19. https://doi.org/10.1186/s13395-020-00236-3

Deng, B., M. Wehling-Henricks, S.A. Villalta, Y. Wang, and J.G. Tidball. 2012. IL-10 triggers changes in macrophage phenotype that promote muscle growth and regeneration. *J. Immunol.* 189:3669–3680. https://doi.org/10.4049/jimmunol.1103180

Duan, J., H. Chung, E. Troy, and D.L. Kasper. 2010. Microbial colonization drives expansion of IL-1 receptor 1-expressing and IL-17-producing γ/δ T cells. *Cell Host. Microbe.* 7:140–150. https://doi.org/10.1016/j.chom.2010.01.005

Fujikado, N., A.O. Mann, K. Bansal, K.R. Romito, E.M.N. Ferre, S.D. Rosenzweig, M.S. Lionakis, C. Benoist, and D. Mathis. 2016. Aire inhibits the generation of a perinatal population of interleukin-17A-producing γδ T cells to promote immunologic tolerance. *Immunity.* 45:999–1012. https://doi.org/10.1016/j.immuni.2016.10.023

Hao, Y., S. Hao, E. Andersen-Nissen, W.M. Mauck, III, S. Zheng, A. Butler, M.J. Lee, A.J. Wilk, C. Darby, M. Zager, et al. 2021. Integrated analysis of multimodal single-cell data. *Cell.* 184:3573–3587.e29. https://doi.org/10.1016/j.cell.2021.04.048

Holtmeier, W., J. Gille, S. Zeuzem, and M. Sinkora. 2010. Distribution and development of the postnatal murine Vδ1 T-cell receptor repertoire. *Immunology.* 131:192–201. https://doi.org/10.1111/j.1365-2567.2010.03290.x

Hoshino, H., J. Lotvall, B.E. Skoogh, and A. Linden. 1999. Neutrophil recruitment by interleukin-17 into rat airways *in vivo*. *Am. J. Respir. Crit. Care Med.* 159:1423–1428. https://doi.org/10.1164/ajrccm.159.5.9806008

Huang, H., H.J. Kim, E.J. Chang, Z.H. Lee, S.J. Hwang, H.M. Kim, Y. Lee, and H.H. Kim. 2009. IL-17 stimulates the proliferation and differentiation of human mesenchymal stem cells: implications for bone remodeling. *Cell Death Differ.* 16:1332–1343. https://doi.org/10.1038/cdd.2009.74

Ismail, A.S., K.M. Severson, S. Vaishnava, C.L. Behrendt, X. Yu, J.L. Benjamin, K.A. Ruhn, B. Hou, A.L. DeFranco, F. Yarovinsky, et al. 2011. Gammadelta intraepithelial lymphocytes are essential mediators of host-microbial homeostasis at the intestinal mucosal surface. *Proc. Natl. Acad. Sci. USA.* 108:8743–8748. https://doi.org/10.1073/pnas.1019574108

Jin, C., G.K. Lagoudas, C. Zhao, S. Bullman, A. Bhutkar, B. Hu, S. Ameh, D. Sandel, X.S. Liang, S. Mazzilli, et al. 2019. Commensal microbiota promote lung cancer development via γδ T cells. *Cell.* 176:998–1013.e16. https://doi.org/10.1016/j.cell.2018.12.040

Kageyama, T., A. Suto, T. Iwamoto, S. Tanaka, K. Suehiro, Y. Yokoyama, A. Saku, S. Furuta, K. Ikeda, K. Suzuki, et al. 2017. IL-21 exacerbates autoimmune myositis by enhancing the accumulation of GM-CSF-producing γδ T cells in the muscle. *ImmunoHorizons.* 1:176–187. https://doi.org/10.4049/immunohorizons.1700053

Kuleshov, M.V., M.R. Jones, A.D. Rouillard, N.F. Fernandez, Q. Duan, Z. Wang, S. Koplev, S.L. Jenkins, K.M. Jagodnik, A. Lachmann, et al. 2016. Enrichr: a comprehensive gene set enrichment analysis web server 2016 update. *Nucleic Acids Res.* 44:W90–W97. https://doi.org/10.1093/nar/gkw377

Kuswanto, W., D. Burzyn, M. Panduro, K.K. Wang, Y.C. Jang, A.J. Wagers, C. Benoist, and D. Mathis. 2016. Poor repair of skeletal muscle in aging mice reflects a defect in local, interleukin-33-dependent accumulation of regulatory T cells. *Immunity.* 44:355–367. https://doi.org/10.1016/j.immuni.2016.01.009

Laan, M., Z.H. Cui, H. Hoshino, J. Lotvall, M. Sjostrand, D.C. Gruenert, B.E. Skoogh, and A. Linden. 1999. Neutrophil recruitment by human IL-17 via C-X-C chemokine release in the airways. *J. Immunol.* 162:2347–2352.

Lafaille, J.J., A. DeCloux, M. Bonneville, Y. Takagaki, and S. Tonegawa. 1989. Junctional sequences of T cell receptor gamma delta genes: implications for γδ T cell lineages and for a novel intermediate of V-(D)-J joining. *Cell.* 59:859–870. https://doi.org/10.1016/0092-8674(89)90609-0

Lahiri, S., H. Kim, I. Garcia-Perez, M.M. Reza, K.A. Martin, P. Kundu, L.M. Cox, J. Selkrig, J.M. Posma, H. Zhang, et al. 2019. The gut microbiota influences skeletal muscle mass and function in mice. *Sci. Transl. Med.* 11. eaan5662. https://doi.org/10.1126/scitranslmed.aan5662

Lee, J.S., C.M. Tato, B. Joyce-Shaikh, M.F. Gulen, C. Cayatte, Y. Chen, W.M. Blumenschein, M. Judo, G. Ayanoglu, T.K. McClanahan, et al. 2015.

Interleukin-23-independent IL-17 production regulates intestinal epithelial permeability. *Immunity*. 43:727–738. https://doi.org/10.1016/j.immuni.2015.09.003

Lepper, C., T.A. Partridge, and C.M. Fan. 2011. An absolute requirement for Pax7-positive satellite cells in acute injury-induced skeletal muscle regeneration. *Development*. 138:3639–3646. https://doi.org/10.1242/dev.067595

Li, F., X. Hao, Y. Chen, L. Bai, X. Gao, Z. Lian, H. Wei, R. Sun, and Z. Tian. 2017. The microbiota maintain homeostasis of liver-resident γδT-17 cells in a lipid antigen/CD1d-dependent manner. *Nat. Commun.* 7:13839. https://doi.org/10.1038/ncomms13839

Liu, L., T.H. Cheung, G.W. Charville, and T.A. Rando. 2015. Isolation of skeletal muscle stem cells by fluorescence-activated cell sorting. *Nat. Protoc.* 10:1612–1624. https://doi.org/10.1038/nprot.2015.110

Londhe, P., and J.K. Davie. 2011. Gamma interferon modulates myogenesis through the major histocompatibility complex class II transactivator, CIITA. *Mol. Cell. Biol.* 31:2854–2866. https://doi.org/10.1128/MCB.05397-11

Londhe, P., and J.K. Davie. 2013. Interferon-gamma resets muscle cell fate by stimulating the sequential recruitment of JARID2 and PRC2 to promoters to repress myogenesis. *Sci. Signal.* 6:ra107. https://doi.org/10.1126/scisignal.2004633

Majumder, S., and M.J. McGeachy. 2021. IL-17 in the pathogenesis of disease: good intentions gone awry. *Annu. Rev. Immunol.* 39:537–556. https://doi.org/10.1146/annurev-immunolan101819-092536

Martin, B., K. Hirota, D.J. Cua, B. Stockinger, and M. Veldhoen. 2009. Interleukin-17-producing gammadelta T cells selectively expand in response to pathogen products and environmental signals. *Immunity*. 31:321–330. https://doi.org/10.1016/j.immuni.2009.06.020

McKenzie, D.R., E.E. Kara, C.R. Bastow, T.S. Tyllis, K.A. Fenix, C.E. Gregor, J.J. Wilson, R. Babb, J.C. Paton, A. Kallies, et al. 2017. IL-17-producing γδ T cells switch migratory patterns between resting and activated states. *Nat. Commun.* 8:15632. https://doi.org/10.1038/ncomms15632

Morton, A.M., E. Sefik, R. Upadhyay, R. Weissleder, C. Benoist, and D. Mathis. 2014. Endoscopic photoconversion reveals unexpectedly broad leukocyte trafficking to and from the gut. *Proc. Natl. Acad. Sci. USA.* 111:6696–6701. https://doi.org/10.1073/pnas.1405634111

Nishimura, D., H. Sakai, T. Sato, F. Sato, S. Nishimura, N. Toyama-Sorimachi, J.W. Bartsch, and A. Sehara-Fujisawa. 2015. Roles of ADAM8 in elimination of injured muscle fibers prior to skeletal muscle regeneration. *Mech. Dev.* 135:58–67. https://doi.org/10.1016/j.mod.2014.12.001

Nueda, M.J., S. Tarazona, and A. Conesa. 2014. Next maSigPro: updating maSigPro bioconductor package for RNA-seq time series. *Bioinformatics*. 30:2598–2602. https://doi.org/10.1093/bioinformatics/btu333

O'Brien, R.L., and W.K. Born. 2015. Dermal γδ T cells - What have we learned? *Cell. Immunol.* 296:62–69. https://doi.org/10.1016/j.cellimm.2015.01.011

Paget, C., M.T. Chow, N.A. Gherardin, P.A. Beavis, A.P. Uldrich, H. Duret, M. Hassane, F. Souza-Fonseca-Guimaraes, D.A. Mogilenko, D. Staumont-Salle, et al. 2015. CD3bright signals on gammadelta T cells identify IL-17A-producing Vgamma6Vdelta1+ T cells. *Immunol. Cell Biol.* 93:198–212. https://doi.org/10.1038/icb.2014.94

Panduro, M., C. Benoist, and D. Mathis. 2018. T_{reg} cells limit IFN-γ production to control macrophage accrual and phenotype during skeletal muscle regeneration. *Proc. Natl. Acad. Sci. USA.* 115:E2585–E2593. https://doi.org/10.1073/pnas.1800618115

Picelli, S., A.K. Bjorklund, O.R. Faridani, S. Sagasser, G. Winberg, and R. Sandberg. 2013. Smart-seq2 for sensitive full-length transcriptome profiling in single cells. *Nat. Methods*. 10:1096–1098. https://doi.org/10.1038/nmeth.2639

Picelli, S., O.R. Faridani, A.K. Bjorklund, G. Winberg, S. Sagasser, and R. Sandberg. 2014. Full-length RNA-seq from single cells using Smart-seq2. *Nat. Protoc.* 9:171–181. https://doi.org/10.1038/nprot.2014.006

Radu, M., and J. Chernoff. 2013. An in vivo assay to test blood vessel permeability. *J. Vis. Exp.* https://doi.org/10.3791/50062

Roark, C.L., M.K. Aydintug, J. Lewis, X. Yin, M. Lahn, Y.S. Hahn, W.K. Born, R.E. Tigelaar, and R.L. O'Brien. 2004. Subset-specific, uniform activation among V gamma 6/V delta 1+ gamma delta T cells elicited by inflammation. *J. Leukoc. Biol.* 75:68–75. https://doi.org/10.1189/jlb.0703326

Sambasivan, R., R. Yao, A. Kissenpfennig, L. Van Wittenberghe, A. Paldi, B. Gayraud-Morel, H. Guenou, B. Malissen, S. Tajbakhsh, and A. Galy. 2011. Pax7-expressing satellite cells are indispensable for adult skeletal muscle regeneration. *Development*. 138:3647–3656. https://doi.org/10.1242/dev.067587

Sandrock, I., A. Reinhardt, S. Ravens, C. Binz, A. Wilharm, J. Martins, L. Oberdorfer, L. Tan, S. Lienenklaus, B. Zhang, et al. 2018. Genetic models reveal origin, persistence and non-redundant functions of IL-17-producing γδ T cells. *J. Exp. Med.* 215:3006–3018. https://doi.org/10.1084/jem.20181439

Schindelin, J., I. Arganda-Carreras, E. Frise, V. Kaynig, M. Longair, T. Pietzsch, S. Preibisch, C. Rueden, S. Saalfeld, B. Schmid, et al. 2012. Fiji: an open-source platform for biological-image analysis. *Nat. Methods*. 9:676–682. https://doi.org/10.1038/nmeth.2019

Segawa, M., S.i. Fukada, Y. Yamamoto, H. Yahagi, M. Kanematsu, M. Sato, T. Ito, A. Uezumi, S. Hayashi, Y. Miyagoe-Suzuki, et al. 2008. Suppression of macrophage functions impairs skeletal muscle regeneration with severe fibrosis. *Exp. Cell Res.* 314:3232–3244. https://doi.org/10.1016/j.yexcr.2008.08.008

Seo, B.R., C.J. Payne, S.L. McNamara, B.R. Freedman, B.J. Kwee, S. Nam, I. de Lázaro, M. Darnell, J.T. Alvarez, M.O. Dellacherie, et al. 2021. Skeletal muscle regeneration with robotic actuation-mediated clearance of neutrophils. *Sci. Transl. Med.* 13. eabe8868. https://doi.org/10.1126/scitranslmed.abe8868

Subramanian, A., P. Tamayo, V.K. Mootha, S. Mukherjee, B.L. Ebert, M.A. Gillette, A. Paulovich, S.L. Pomeroy, T.R. Golub, E.S. Lander, et al. 2005. Gene set enrichment analysis: a knowledge-based approach for interpreting genome-wide expression profiles. *Proc. Natl. Acad. Sci. USA.* 102:15545–15550. https://doi.org/10.1073/pnas.0506580102

Sutton, C.E., S.J. Lalor, C.M. Sweeney, C.F. Brereton, E.C. Lavelle, and K.H. Mills. 2009. Interleukin-1 and IL-23 induce innate IL-17 production from γδ T cells, amplifying Th17 responses and autoimmunity. *Immunity*. 31:331–341. https://doi.org/10.1016/j.immuni.2009.08.001

Teixeira, C.F., S.R. Zamuner, J.P. Zuliani, C.M. Fernandes, M.A. Cruz-Hofling, I. Fernandes, F. Chaves, and J.M. Gutierrez. 2003. Neutrophils do not contribute to local tissue damage, but play a key role in skeletal muscle regeneration, in mice injected with Bothrops asper snake venom. *Muscle Nerve*. 28:449–459. https://doi.org/10.1002/mus.10453

Tidball, J.G. 2017. Regulation of muscle growth and regeneration by the immune system. *Nat. Rev. Immunol.* 17:165–178. https://doi.org/10.1038/nri.2016.150

Tomura, M., N. Yoshida, J. Tanaka, S. Karasawa, Y. Miwa, A. Miyawaki, and O. Kanagawa. 2008. Monitoring cellular movement in vivo with photoconvertible fluorescence protein "Kaede" transgenic mice. *Proc. Natl. Acad. Sci. USA.* 105:10871–10876. https://doi.org/10.1073/pnas.0802278105

Tonkin, J., L. Temmerman, R.D. Sampson, E. Gallego-Colon, L. Barberi, D. Bilbao, M.D. Schneider, A. Musaro, and N. Rosenthal. 2015. Monocyte/macrophage-derived IGF-1 orchestrates murine skeletal muscle regeneration and modulates autocrine polarization. *Mol. Ther.* 23:1189–1200. https://doi.org/10.1038/mt.2015.66

Varga, T., R. Mounier, A. Patsalos, P. Gogolak, M. Peloquin, A. Horvath, A. Pap, B. Daniel, G. Nagy, E. Pintye, et al. 2016. Macrophage PPARγ, a lipid activated transcription factor controls the growth factor GDF3 and skeletal muscle regeneration. *Immunity*. 45:1038–1051. https://doi.org/10.1016/j.immuni.2016.10.016

Villalta, S.A., B. Deng, C. Rinaldi, M. Wehling-Henricks, and J.G. Tidball. 2011. IFN-γ promotes muscle damage in the mdx mouse model of Duchenne muscular dystrophy by suppressing M2 macrophage activation and inhibiting muscle cell proliferation. *J. Immunol.* 187:5419–5428. https://doi.org/10.4049/jimmunol.1101267

Villalta, S.A., W. Rosenthal, L. Martinez, A. Kaur, T. Sparwasser, J.G. Tidball, M. Margeta, M.J. Spencer, and J.A. Bluestone. 2014. Regulatory T cells suppress muscle inflammation and injury in muscular dystrophy. *Sci. Transl. Med.* 6:258ra142. https://doi.org/10.1126/scitranslmed.3009925

Wei, Y.L., A. Han, J. Glanville, F. Fang, L.A. Zuniga, J.S. Lee, D.J. Cua, and Y.H. Chien. 2015. A highly focused antigen receptor repertoire characterizes γδ T cells that are poised to make IL-17 rapidly in naive animals. *Front. Immunol.* 6:118. https://doi.org/10.3389/fimmu.2015.00118

Wilharm, A., Y. Tabib, M. Nassar, A. Reinhardt, G. Mizraji, I. Sandrock, O. Heyman, J. Barros-Martins, Y. Aizenbud, A. Khalaileh, et al. 2019. Mutual interplay between IL-17-producing gammadeltaT cells and microbiota orchestrates oral mucosal homeostasis. *Proc. Natl. Acad. Sci. USA.* 116:2652–2661. https://doi.org/10.1073/pnas.1818812116

Witowski, J., K. Pawlaczyk, A. Breborowicz, A. Scheuren, M. Kuzlan-Pawlaczyk, J. Wisniewska, A. Polubinska, H. Friess, G.M. Gahl, U. Frei, et al. 2000. IL-17 stimulates intraperitoneal neutrophil infiltration through the release of GRO alpha chemokine from mesothelial cells. *J. Immunol.* 165:5814–5821. https://doi.org/10.4049/jimmunol.165.10.5814

Wu, L., X. Chen, J. Zhao, B. Martin, J.A. Zepp, J.S. Ko, C. Gu, G. Cai, W. Ouyang, G. Sen, et al. 2015. A novel IL-17 signaling pathway controlling keratinocyte proliferation and tumorigenesis via the TRAF4-ERK5 axis. *J. Exp. Med.* 212:1571–1587. https://doi.org/10.1084/jem.20150204

Wurbel, M.A., M. Malissen, D. Guy-Grand, E. Meffre, M.C. Nussenzweig, M. Richelme, A. Carrier, and B. Malissen. 2001. Mice lacking the CCR9 CC-chemokine receptor show a mild impairment of early T- and B-cell development and a reduction in T-cell receptor gammadelta(+) gut intraepithelial lymphocytes. *Blood*. 98:2626–2632. https://doi.org/10.1182/blood.v98.9.2626

Ye, P., F.H. Rodriguez, S. Kanaly, K.L. Stocking, J. Schurr, P. Schwarzenberger, P. Oliver, W. Huang, P. Zhang, J. Zhang, et al. 2001. Requirement of interleukin 17 receptor signaling for lung CXC chemokine and granulocyte colony-stimulating factor expression, neutrophil recruitment, and host defense. *J. Exp. Med*. 194:519–527. https://doi.org/10.1084/jem.194.4.519

Zepp, J.A., J. Zhao, C. Liu, K. Bulek, L. Wu, X. Chen, Y. Hao, Z. Wang, X. Wang, W. Ouyang, et al. 2017. IL-17A-induced PLET1 expression contributes to tissue repair and colon tumorigenesis. *J. Immunol*. 199:3849–3857. https://doi.org/10.4049/jimmunol.1601540

Zhao, J., X. Chen, T. Herjan, and X. Li. 2020. The role of interleukin-17 in tumor development and progression. *J. Exp. Med*. 217:e20190297. https://doi.org/10.1084/jem.20190297

JEM

Supplemental material

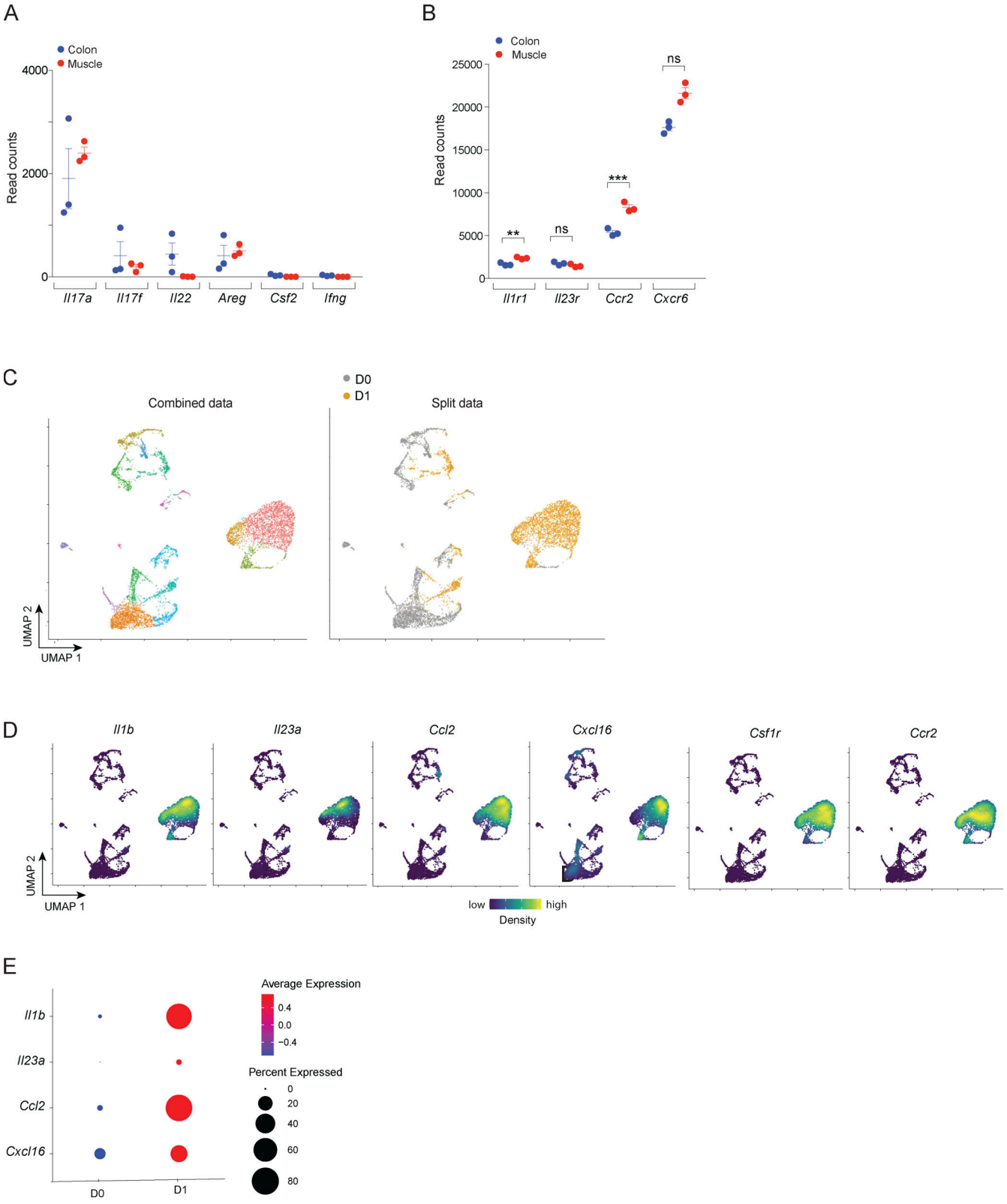

Figure S1. **Transcriptional analysis of factors involved in IL-17A⁺ γδT cell accumulation and function. (A and B)** RNA-seq quantification of key transcripts by Vγ6⁺ T cells sorted from muscle 3 d after injury or from the colonic lamina propria. From three independent mice. **(C–E)** Reanalysis of whole-muscle scRNA-seq data obtained from uninjured mice or 24 h after injury (Baht et al., 2020). **(C)** Left: 2D UMAP plot of data from two time points combined. Right: Cell distribution across the two time points. **(D and E)** Density plots (D) and bubble plots (E) of the average transcript expression for cytokines and chemokines known to be crucial for γδT cell proliferation and recruitment. Mean ± SEM. ns, not significant. **, P < 0.01; ***, P < 0.001, by unpaired *t* test.

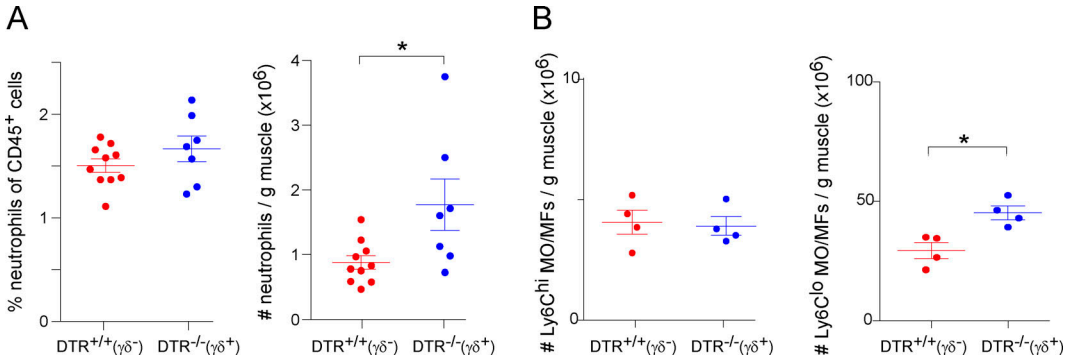

Figure S2. **γδT cells promote early inflammation after muscle injury. (A)** Flow cytometric quantification of fractional representation (left) and numbers (right) of muscle neutrophils 3 d after CTX-induced injury. Data obtained from two independent experiments. **(B)** Right: Flow cytometric quantification of the numbers of Ly6C^{hi} MO/MFs in muscle 3 d after injury. Left: Same as B, except numbers of Ly6C^{lo} MO/MFs were quantified. Data are representative of two independent experiments. Mean ± SEM. *, P < 0.05 by unpaired *t* test.

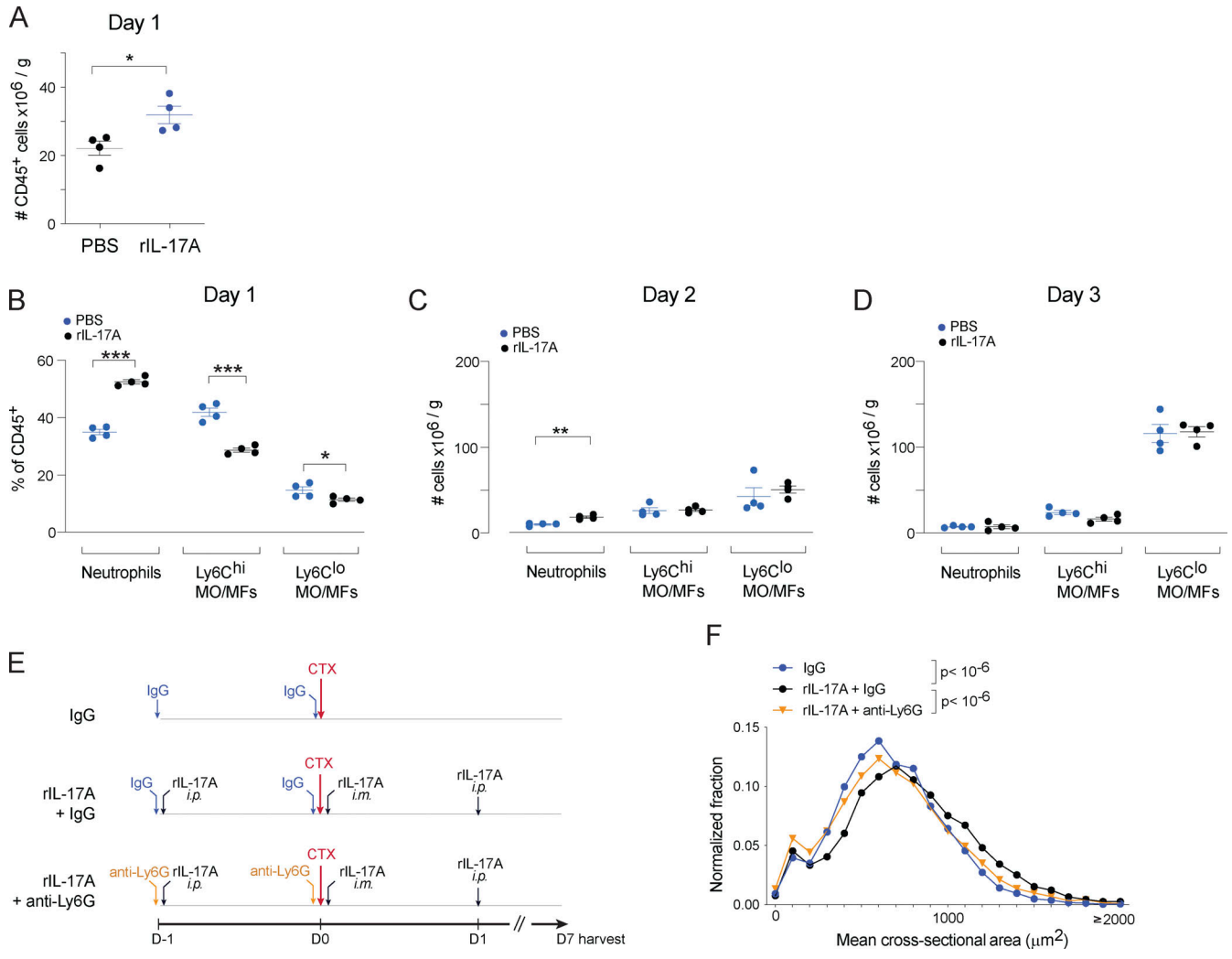

Figure S3. **IL-17A boosts early inflammation after acute injury. (A)** Flow cytometric quantification of CD45$^+$ immunocyte numbers 1 d after CTX. **(B)** Flow cytometric analysis of the fractional representation of myeloid cell populations in hindlimb muscle at 1 d after CTX. **(C and D)** Flow cytometric quantification of myeloid cell populations in hindlimb muscle at 2 d (C) or 3 d (D) after injury. **(E)** Schematic of antibody-mediated depletion of neutrophils along with injury in conjunction with rIL-17A treatment. **(F)** Distribution of cross-sectional areas of individual centrally nucleated muscle fibers on H&E sections (*n* = 3–5 mice per group). Samples with <10% injured area in TA muscles were excluded from the analysis. Statistical analysis of frequency distributions was performed using *t* test of weighted sums. Data in A, B, and D are representative of three independent experiments, and in C, E, and F, of one independent experiment. Mean ± SEM. *, P < 0.05 **, P < 0.01; ***, P < 0.001 by unpaired *t* test unless otherwise indicated.

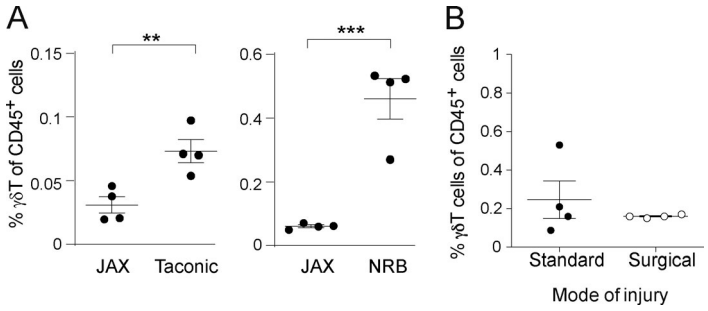

Figure S4. **The microbiota controls accumulation of muscle γδT cells. (A)** Flow cytometric quantification of the fractional representation of γδT cells in hindlimb muscle 3 d after CTX in mice from various housing facilities. **(B)** Same as A, but from mice that underwent either standard or sterile surgical injury. Jax, Jackson Laboratory; NRB, New Research Building at Harvard Medical School. Mean ± SEM. **, P < 0.01; ***, P < 0.001, by unpaired *t* test.

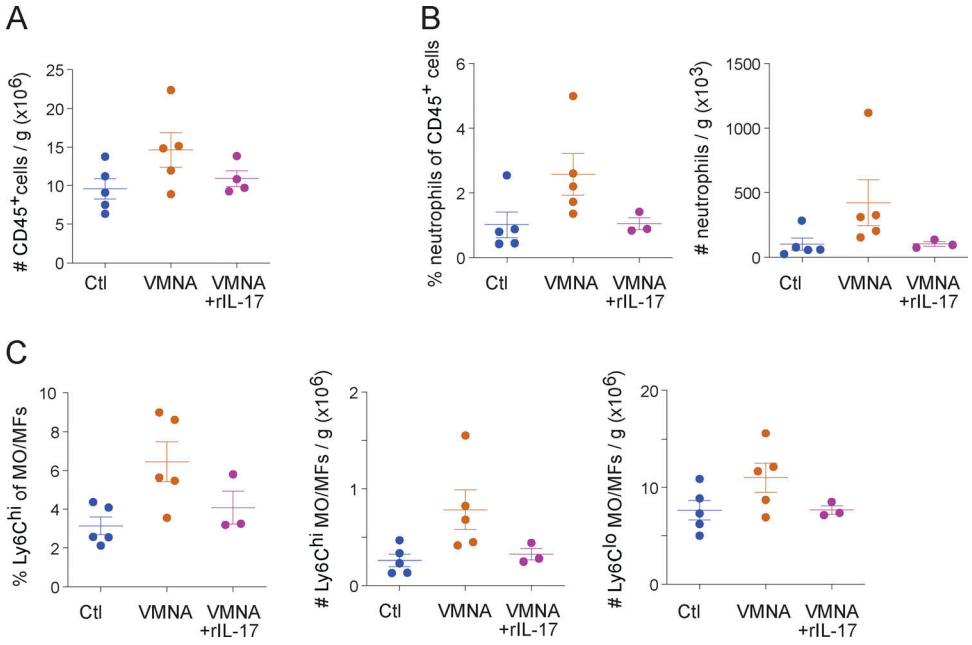

Figure S5. **The microbiota controls resolution of inflammation after muscle injury. (A)** Flow cytometric quantification of total muscle immunocyte numbers 7 d after injury. **(B)** Flow cytometric analysis of neutrophil fractional representation (left) and numbers (right) in hindlimb muscles 7 d after injury. **(C)** Flow cytometric analysis of MO/MF subsets in hindlimb muscles 7 d after injury. Left: Fractional representation of Ly6C^{hi} MO/MFs. Center: Numbers of Ly6C^{hi} MO/MFs. Right: Numbers of Ly6C^{lo} MO/MFs. Ctl, control. Mean ± SEM. No significant differences according to one-way ANOVA with Bonferroni post hoc test.